UC Irvine
UC Irvine Electronic Theses and Dissertations

Title

Machine Learning of PEM Fuel Cell Degradation: Artificial Neural Network and Long Short-Term Memory Recurrent Neural Network

Permalink

https://escholarship.org/uc/item/3m02d442

Author

Nourizadeh, Amirhossein

Publication Date

2023

Peer reviewed|Thesis/dissertation

UNIVERSITY OF CALIFORNIA,
IRVINE

Machine Learning of PEM Fuel Cell Degradation: Artificial Neural Network and Long Short-Term Memory Recurrent Neural Network

THESIS

submitted in partial satisfaction of the requirements
for the degree of

MASTER OF SCIENCE

in Mechanical and Aerospace Engineering

by

Amirhossein Nourizadeh

Thesis Committee:

Professor Yun Wang, Chair
Professor Manuel Gamero-Castaño
Professor Feng Liu

2023

TABLE OF CONTENTS

LIST OF FIGURES

LIST OF TABLES

ACKNOWLEDGEMENTS

ABSTRACT OF THE THESIS

Machine Learning of PEM Fuel Cell Degradation: Artificial Neural Networks and Long Short-Term Memory Recurrent Neural Networks

by

Amirhossein Nourizadeh

Master of Science

in Mechanical and Aerospace Engineering

University of California, Irvine, 2023

Professor Yun Wang, Chair

Proton exchange membrane fuel cells' (PEMFCs') degradation is a main problem that must be solved for their commercialization. In this thesis, we employ data-driven prognostic models to forecast PEMFC voltage degradation utilizing artificial neural networks (ANN), deep neural networks (DNN), and long short-term memory (LSTM) techniques. The suggested models are developed and tested using experimental information obtained through PEMFC stack testing, and their performance is assessed using a variety of metrics, such as root mean square error (RMSE). The findings show that the DNN technique performs better than the other methods, indicating that the model can reliably and precisely forecast the PEMFC stack voltage decline. In addition, we examined the models' performance in terms of the neural network designs' number of neurons and layers. The results demonstrate a trade-off between prediction accuracy and computational complexity, with an increase in neurons and layers able to enhance prediction accuracy. In conclusion, the suggested data-driven prognostic models may offer precise and

trustworthy forecasts of PEMFC stack voltage degradation, which can aid in optimizing system design and operation. In order to improve the precision and effectiveness of the prediction process, future research can concentrate on investigating the applicability of these models to specific degradation modes, such as catalyst and membrane degradation, and developing more sophisticated data-driven prognostic models. Moreover, combining data-driven and physics-based models can offer a thorough strategy for PEMFC degradation prognostics.

Chapter 1: Introduction

1.1 PEMFC

As a result of the widespread societal use of fossil fuels, which has led to issues like air pollution and global warming that have a significant negative impact on the environment, environmental issues have grown more and more serious in recent decades. Global energy-related CO_2 emissions will rise from 32.3 billion metric tonnes in 2012 to 35.6 billion metric tonnes in 2020 and to 43.2 billion metric tonnes in 2040, predicts the International Energy Outlook 2016 (IEO 2016) Reference case report from the U.S. Energy Information Administration (EIA). This is a predictable increase of 40% in carbon dioxide emissions. If various nations around the world gave this serious consideration, it might not happen [1].

The globe has seen rising global energy demand, rising fossil fuel costs, and a rise in air pollution due to rising greenhouse gas emissions during the last few decades. All of these have significantly pushed us forward in the realm of renewable energy research and development. One of the most promising clean energy technologies for supplying electrical energy in stationary or mobile applications is fuel cell.

Fuel cells are electrochemical energy conversion devices that are totally eco-friendly if the hydrogen (the fuel) is generated entirely from renewable energy sources. It is a very promising energy source for the future due to its low carbon dioxide emissions, high energy density, and lack of reliance on fossil fuels. Water and heat are the only byproducts of the electrochemical interaction between hydrogen and oxygen in the air that proton exchange membrane fuel cell (PEMFC) can use to generate energy [Wang, Y., & Chen, K. S. (2013). PEM fuel cells: thermal and water management fundamentals. Momentum Press.].

This energy conversion is 100 percent environmentally benign if the hydrogen is generated using sources of renewable energy. Due to their potential as alternatives for sustainable energy solutions in the near future, PEMFCs are gaining more and more attention. Moreover, the absence of moving components in PEMFC constructions assures the dependability and compactness of fuel cell systems.

When we utilized the term "PEMFC," we may have been referring to PEMFC stacks or PEMFC single cells. To achieve the required energy, a PEMFC stack often consists of dozens or even hundreds of single cells. A PEMFC stack is created by electrically connecting these identical single cells in series.

1.1.1 The structure of PEMFC

A PEMFC single cell's typical architecture is seen in Figure 1 [1, 2]. Air (oxygen) is delivered to the copper electrode, and hydrogen is fed to the anode electrode throughout the operation. The gas diffusion layer subsequently allows the hydrogen and oxygen to pass through to the catalyst layer on every side. The existence of platinum catalyst at the anode catalyst layer causes the hydrogen molecules to become disassociated from protons and electrons. Next, to create the electrical current, the protons move through to the humidified polymer electrolyte (membrane) from the anode electrode to the copper electrode. During this time, the electrons are transported through the external circuit from the anode to the cathode. Protons, electrons, and oxygen molecules are eventually united at the cathode catalyst layer to create water and heat as byproducts.
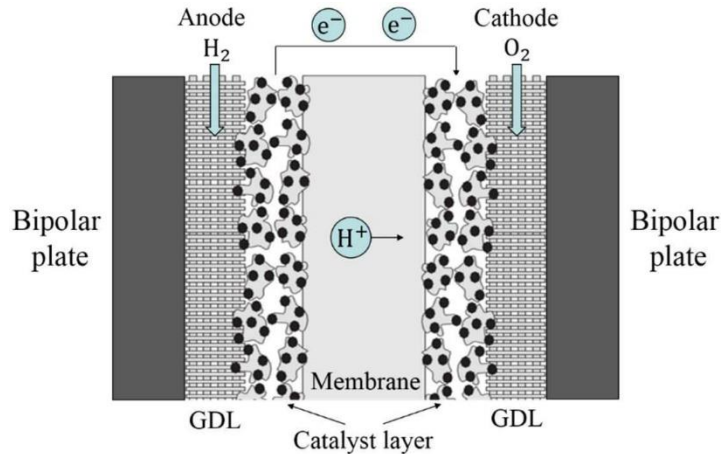
Figure 1 PEMFC single cell's design [1].

Each individual cell is made up of the following structural components:

1.   Polymer electrolyte membrane

Inside a cell, the polymer electrolyte membrane (PEM), also known as the proton exchange membrane, controls proton transmission, reaction separation processes, and electrode electrical insulation. Proton conduction throughout the membrane is made easier by the polymer electrolyte, which enables the single cell to operate with a relatively thin membrane while until withstanding high pressures [3].

The PEMFC membranes are a type of ionomer that includes a significant amount of polymer ions, often the sulphonic end groups. Protons can only penetrate a membrane when they are carried by hydrophilic ionic end groups. Previously, a variety of membrane varieties were employed, but today, the perfluoro sulfonic acid (often referred to as PFSA in the literature) membranes are utilized extensively in PEMFCs. It is most frequently referred to as a membrane of the Nafion type. The PFSA's structure might, on the one hand, provide stability in the acidic medium brought on by the hydrogen ions contained inside it, and, on

the other hand, could also act as a conduit for the hydrogen ions to diffuse from the anode to the cathode. Its thickness typically ranges from 10 to 50 microns for PEMFCs of the present [4]. Water molecules would prefer to aggregate and form clusters on the hydrophilic end groups of the PFSA whenever the membrane absorbs water. These water clusters might then serve as routes for protons moving from the anode to the cathode. With greater water absorption, the membrane's proton conductivity would increase.

If the membrane can withstand these two conditions, it is often said to be functioning adequately. The pressured gases in the anode and cathode electrodes should be physically separated from one another with almost no gas crossing. Furthermore, it must remain chemically stable in adverse circumstances like those brought on by the activity of catalysts, temperature swings, extremely high temperatures, or assaults from oxidative radicals that were first created by H_2O_2. In further detail, the radicals are either synthesized in the membrane, where they are made on the surface of the precipitated platinum particles, or from the incomplete chemical interactions between the hydrogen and oxygen on the cathode electrode. The optimal membrane for the PEMFC stack should hence, generally, have great proton conductivity, high chemical and thermal stability, mechanical strength, flexibility, almost no gas penetration, cheap cost, and accessibility.

Several kinds of membranes utilized in PEMFCs have been covered in the literature [5]. It enables us to recognize the various membrane types, as well as their characteristics and information on membrane breakdown. Actuality, the lifetime of a fuel cell is closely tied to how durable its membrane is [6]. We must acknowledge the aging processes that contribute to the decline in membrane performance. Yet, since membrane degradations can

be brought on by a variety of operational conditions, it is difficult to separate and identify the different membrane degradation pathways. These elements typically have combined effects on membranes.

2.   Catalyst layer

The two slim catalyst layers (CL) are coated on either side of the PEM. In the CLs, the electrochemical reactions take occur. Traditional CL is mostly made of platinum nanoparticles supported by carbon surfaces and a combination of ionomer in a predetermined proportion [Wu, J., Liu, H., Song, Y., & Wang, Y. (2022). A modeling study of PEM fuel cells with novel catalyst monolayers under low platinum loading. Journal of Materials Chemistry A, 10(8), 4076-4086.]. This layer's carbon surface would allow for electron conductivity and platinum dispersion. The ionomer, which theoretically maintains the structural integrity of the catalyst layer, has several distinct hydrophilic and hydrophobic fields that allow reactants and protons to reach the platinum nanoparticles' active sites, where reactions may take place [Wang, Y., & Feng, X. (2009). Analysis of the reaction rates in the cathode electrode of polymer electrolyte fuel Cells: II. Dual-Layer electrodes. Journal of The Electrochemical Society, 156(3), B403.]. As seen in *Figure 1*, the reduction process of oxygen occurs on the right side (the cathode side), while the oxidation reaction of hydrogen occurs on the active sites of the catalyst layer on the left (the anode side).

3.   Gas diffusion layer (GDL)

The gas diffusion layer is located between the CL and the bipolar plate (BP). Nonwoven carbon paper and woven carbon cloth are the two primary types of GDLs. It enables the hydrogen and oxygen (or air) from both sides of the cell to diffuse into the layers

of the catalyst, where the electrochemical reaction would occur. In particular, diffusion and convection-diffusion are the two ways that reactants diffuse into the compressed GDL. They are determined by the BP's flow field channels' channel design and the shape of the GDL pores.

Polytetrafluoroethylene (PTFE) hydrophobic coating is often applied to GDLs to facilitate the efficient transmission of liquid water and reactive gases. GDL's hydrophobic properties are crucial to the overall cell's ability to handle water. The ratio of hydrophilic to hydrophobic regions on the surface of the GDL will have a significant impact on how efficiently gas and water are transported [7]. The catalyst layer and membrane's water management are made easier by the PTFE treatment applied to GDL's porous surface.

It may permit reactant gases and water vapor to diffuse through its pores together, ensuring that the membrane is sufficiently wet. Also, having the ability to remove any liquid water formed on the cathode side from each cell is beneficial in the interim because it keeps the water from obstructing the pores leading to the active sites. Furthermore, the bipolar plates and catalyst layer are electrically coupled to GDL. The exchange of electrons between the active sites and the bipolar plates may be guaranteed as a result.

The GDLs in PEMFC typically operate in a high-pressing stress environment [Zheng, B., Wang, Z., & Wang, Y. (2022). Porous media flow field for polymer electrolyte membrane fuel cell: Depression of gas diffusion layer intrusion, deformation, and delamination. International Journal of Energy Research, 46(14), 20039-20049.]. Thus, the GDL must be robust and offer adequate air permeability when compressed.

4.   Bipolar plates

The reaction gases must be supplied to the electrodes with flow field channels on the bipolar plates in order for the electrodes to function. As well, the bipolar plates' capacity to electrically interact with several cells in series makes them crucial for multi-cell arrangements. Furthermore, they may functionally support the cells in a compressed and compact arrangement, increasing operating reliability. In reality, the effectiveness of gas supply depends greatly on the configuration of the flow field channels and two-phase flow [Cho, S. C., & Wang, Y. (2014). Two-phase flow dynamics in a micro channel with heterogeneous surfaces. International Journal of Heat and Mass Transfer, 71, 349-360.].

Significant electrical conductivity, high corrosion resistance, a high degree of mechanical strength, minimal electrical or thermal contact resistance, low permeability of reactant gases, and low friability are all qualities that bipolar plates should possess [8, 9]. Bipolar plates can be made from a range of materials, including metal, composite, and graphite, in order to satisfy these requirements [Wang, Y., Pham, L., de Vasconcellos, G. P. S., & Madou, M. (2010). Fabrication and characterization of micro PEM fuel cells using pyrolyzed carbon current collector plates. Journal of Power Sources, 195(15), 4796-4803.]. The anti-corrosion capacity and the contact resistance of the material used in bipolar plates would constantly require being balanced in study. They must select those with the lowest resistance and the highest anti-corrosion capacity.

The cells are arranged in succession as illustrated in *Figure 2* in order to provide an adequate electric power output. As we can observe in the *Figure 2*, any individual cell is formed by compressing the MEA into a small space between the two parts of the bipolar

plates. Indeed, throughout PEMFC operation, the reactant gases in the flow field channels might diffuse to the anode or cathode electrode of each cell and enable the electrochemical reactions. This is because hydrogen and oxygen are supplied to either side of the bipolar plates.
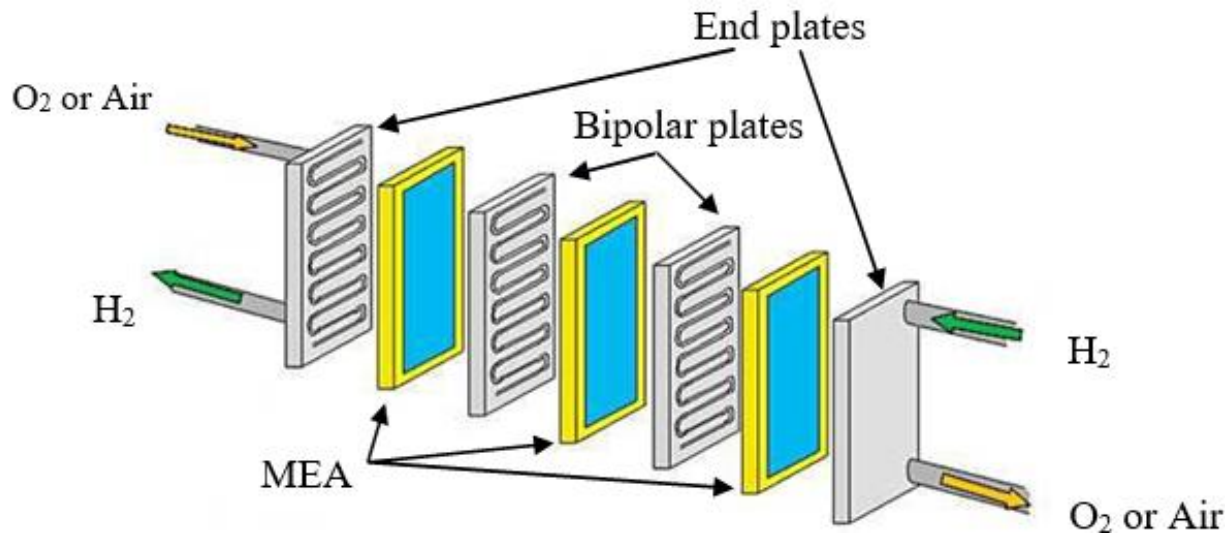
Figure 2 A PEMFC single cell's design[9].

1.1.2 The system of PEMFC

Auxiliaries would always be required for the PEMFC stack to produce power. A PEMFC system is the general term for the system that includes the stack and auxiliaries *Figure 3*. The auxiliary can often be divided into five subsystems:

➢   Reactant supply subsystem

➢   Heat management subsystem

- ➢ Water management subsystem

- ➢ Power conditioning subsystem

- ➢ Power management subsystem
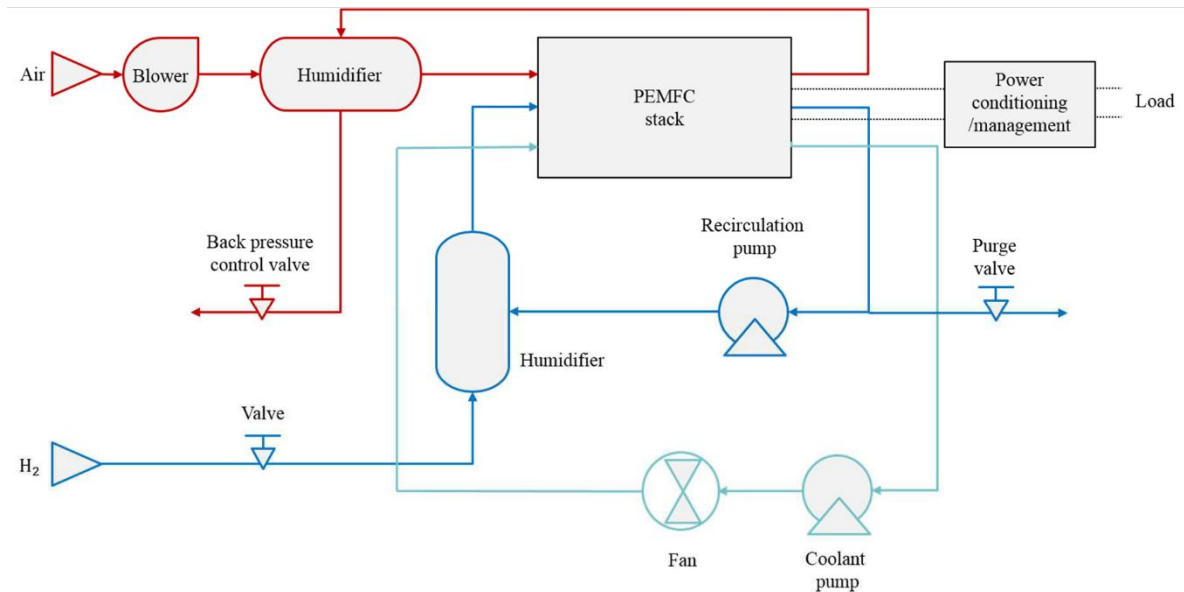
Figure 3 An example of PEMFC system setup.

I. Reactant supply subsystem

The hydrogen and air supply subsystems often make up the reactant supply subsystem.

The hydrogen supply subsystem's goal is to regulate the anode's hydrogen pressure and flow rate. A pressurized hydrogen tank linked to the anode by a pressure reduction valve and a pressure control valve typically makes up the hydrogen supply subsystem. When the hydrogen outlet is blocked and the anode is operating in a dead-end mode, all hydrogen delivered through

the channels are used up by the fuel cells. The vent valve at the anode outlet regularly opens the hydrogen exit for purging to release treated wastewater, stored contaminants, or

nitrogen diffused from the air on the cathode side. So, when the anode is operating in flow-through mode, a recirculation pump device would be used to return the hydrogen from the outlet to the hydrogen intake.

A blower or air compressor that can introduce pressured air into the cathode from the environment typically makes up the air supply subsystem. Its goal is to deliver air at a specific flow rate to guarantee the PEMFC stack is operating properly. At the cathode circuit output, a pressure valve controls the pressure. Typically, a 2.5 bar pressure is applied to the cathode side in order to increase output power. Nevertheless, the power required for the compressor at the system level must be matched with this power enhancement from the stack level.

II.   Heat management subsystem

The stack cooling system and the reactant heating system make up the heat management subsystem. In actuality, the optimal operating temperature range for PEMFCs would be between 60 and 80°C. Hence, a PEMFC system's efficiency and a heat management subsystem's performance are closely associated. In some circumstances, the heat produced as a byproduct might be recycled for additional uses, such as heating the reactant gases at the entrance.

III.   Water management subsystem

To keep the PEMFC operating in an effective condition, water management in the PEMFC system is crucial. The PEMFC stack or system can avoid unintended degradation with proper water management. On the cathode side, the oxygen reduction process results in the production of water. The quantity of water generated on the cathode side would be excessive

in some circumstances, such as those with high current output profiles, and this might affect the operation of the PEMFC by obstructing the GDL. At times, if the reactant gases are not correctly humidified, the PEMFC, particularly the membrane, might get dehydrated in a low current output profile. The effectiveness of the PEMFC would likewise be affected by this. As a result, the water management subsystem is crucial since the efficiency of the PEMFC is highly associated with its performance. The majority of the time, the water management is carried out by active or passive exchange humidifiers between the reactant gas inlets and outlets.

These humidifiers allow for the regulation of the reactant gas's humidity as well as the removal of extra water from the electrodes.

Since the relative humidity levels in the various PEMFC components are connected and may be affected by operational factors like temperature and load change, managing water is a difficult issue. Due to a change in reactant stoichiometry, the humidification level may also have an impact on the PEMFC's efficiency. To best meet the load requirement, the ideal humidity level could not be compatible with an effective flow level of the reactant gases.

There are typically three methods for reactant humidification:

a)   Gas bubbling:

Gas bubbling is a technique that is often applied in a laboratory setting rather than a business setting. The gases would be bubbling at a controlled temperature through a water pipe. In this instance, the temperature would affect and regulate how humid the reactant gases were. Nonetheless, under some circumstances, the humidified reactant gases might still include liquid water.

b)   Direct vapor injection:

Typically, to do this, moisture mist is injected into the reactant gases. A source of heat would be utilized to create fine water vapor to enhance the humidification quality. The quantity of injected moisture is the only factor that affects the humidification rate.

c)   Water exchange through permeable material:

In this scenario, a membrane made of a permeable material like Nafion would be used. Liquid water would pass through the membrane's surface on one side, while reactant gases would move across it on the other side and get humidified as a result of the membrane's water diffusion. The temperature of the water flow can be used to regulate the amount of reactant gas humidification.

IV.   Power conditioning subsystem

Several operational characteristics, including the gas humidification level, gas flow rate, stoichiometry, stack temperature distribution, membrane hydration level, current density, etc., may have an impact on the voltage of each individual PEMFC cell. As a result, before being provided to the load demand, the PEMFC stack's output voltage needs to be controlled.

Regulators for DC/DC or DC/AC are the most common components of the power conditioning subsystem. Transformers and DC/DC or DC/AC coupling may both increase the PEMFC stack's output voltage range and provide electrical isolation between the stack and the load. There would likely be more than one regulator conditioning the PEMFC output in the system since the regulated output voltage might often be employed by the load or the system auxiliaries.

V.   Power management subsystem

In actuality, the PEMFC system is integrated into the power generation system through the power management subsystem. The power management subsystem is typically installed in a working environment which also includes additional energy output or storage elements, such as battery packs or supercapacitors. There wouldn't be a requirement for a power management module in this scenario because the PEMFC stack would be able to provide the entire load if no other energy sources were present. Nevertheless, it is required to construct a power management subsystem within and distribute the output power as appropriate if the system has additional energy sources, such as in a hybrid or electric vehicle situation.

1.1.3 Principles of PEMFC operation

In essence, the transferred chemical energy from the electrochemical processes that took place on the electrodes is what produces the electricity from a functional PEMFC. It would consist of two half-electrochemical reactions occurring on all the electrodes in PEMFC:

In the anode CL:

$$2H_2 \rightarrow 4H^+ + 4e^- \tag{1}$$

In the cathode CL:

$$O_2 + 4H^+ + 4e^- \rightarrow 2H_2O \tag{2}$$

Overall:

$$2H_2 + O_2 \rightarrow 2H_2O \tag{3}$$

The difference between the enthalpies of the products and the reactants is the enthalpy of this overall reaction:

$$\Delta H = H_{H2O} - H_{H2} - 12 H_{O2} = -286 kJ \tag{4}$$

This exothermic reaction releases 286kJ of energy per mole of H_2 which is used throughout the whole process, as indicated by the negative value in the equation. This quantity of released enthalpy is based on the assumption that the water is released in liquid form at 25°C under the conditions of 1 atm.

Enthalpy cannot entirely be transformed into energy, though. Just a portion of the 286kJ released per mole H_2 consumed throughout processing could be turned to electricity because some of the inherent enthalpies cannot be transformed into work. The Gibbs free energy, or ΔG, is this component of energy, in which:

$$\Delta G = \Delta H - T\Delta S \tag{5}$$

The irreversible losses that occur throughout an electrochemical reaction are represented by ΔS, while the reaction temperature in the cell is represented by T. ΔS would vary depending on the reactant's temperature and pressure during operation. According to [10], each mole of hydrogen burned at 25°C under the conditions of atmospheric pressure results in a Gibbs free energy of -237.34kJ of the total available energy in the whole process. Similar to the enthalpy, the negative value indicates that energy is being released during the reaction in this case.

Charge and potential are the components of electrical work, and the theoretical potential that may be generated from this energy is:

$$E_{standard} = \frac{-\Delta G}{nF} = \frac{237.34\ kJ/mol}{2 \times 96485\ As/mol} = 1.23\ V \qquad (6)$$

The number of electrons involved in the whole process for every mole of hydrogen used is denoted by the symbol n, and the faraday constant, F, has a value of 96485 (C/mol). The voltage obtained under normal conditions is 1.23V. In reality, electrochemically, if it weren't operating under normal conditions, the electrodes' potential would depart from 1.23V:

$$E = E_{standard} - \frac{RT}{nF} \ln \left(\frac{a_{H_2O}}{a_{H_2} \cdot a_{O_2}^{0.5}} \right) \qquad (7)$$

In the above equation, a represents of various species' activities. Nevertheless, the fuel cell would often have variable operating losses, which would typically result in a significantly lower power supply when compared to this amount.

The losses [2] may typically be divided into three categories:

1)   Activation losses:

The electrode kinetics must deliver the required activation energy during the electrochemical process in order to produce continuous electrical current, which results in activation losses. Both the anode and cathode electrodes sides experienced losses, however the cathode side losses were significantly more than the anode side losses. This is because the oxygen reduction reaction is far more difficult than the hydrogen oxidation reaction, which occurs on the anode side.

Fundamentally, the Tafel equation on the electrodes might be used to get the activation loss, and the following formulation could be used:

$$V_{act} = \frac{RT}{\alpha F} \ln\left(\frac{i}{i_0}\right) \tag{8}$$

In the Eq. (8), i is the current density, i0 is the exchange current density on the electrode, and α is the transfer coefficient. It could take the form of [2]:

$$i_0 = i_0^{ref} a_c L_c \left(\frac{P_{O_2}}{P_{O_2}^{ref}}\right)^\lambda exp\left(-\frac{E_c}{RT}\left(1 - \frac{T}{T_{ref}}\right)\right) \tag{9}$$

P_{O_2} and $P_{O_2}^{ref}$ are the actual and reference of partial pressures of oxygen in the cathode electrode, respectively. λ is the pressure coefficient. E_c is the activation energy on the cathode electrode for the oxygen reduction process on the catalyst. T and T_{ref} are the actual and reference temperatures, respectively. The loss of platinum on the catalyst layer (L_c) would cause the exchange current density for a PEMFC to decrease during a sufficient period of time. The ac would decrease with time while running under various circumstances, as indicated in the Eq. (9).

2)   Ohmic losses

The resistance to the passage of the ions in the proton electrolyte membrane or of the electrons in the electrically conductive components of the fuel cell, which include the bipolar plates, GDL, etc., is what causes the ohmic losses. As the resistance of every electrically conducting component is almost constant throughout the operation, the quantity of losses is directly proportional to the current.

$$V_{ohmic} = iR_i \tag{10}$$

16

In the above Eq., the internal resistance of the whole cell makes up R_i. The long-term operation would result in an enhancement in R_i, which would eventually result in an enhancement in PEMFC's ohmic losses.

3) Concentration losses

When the reactant gases are used quickly, concentration losses typically occur. The pressure at the reaction site differs from the reactant pressure in the flow field channel due to the diffusivity limitations of various gases in the GDL and bipolar plates. This occurs particularly under conditions of greater output current because, under these conditions, the actual pressure at reaction sites would be significantly lower than the reactant pressure in the flow field channel. Typically, the empirical expression of the concentration loss is:

$$V_{conc} = \frac{RT}{nF} \ln \left(\frac{i_{limit}}{i_{limit} - 1} \right) \tag{11}$$

Here, the limiting current density is denoted by the symbol i_{limit}. Owing to the diffusion constraint from the flow field channel to the surface of the electrode, it is the maximum current density that the electrode can supply.

The output performance of the PEMFC stack would be significantly impacted by these three voltage losses that occurred across each cell. In zones I, II, and III, respectively, of *Figure 4*, they are dominant.
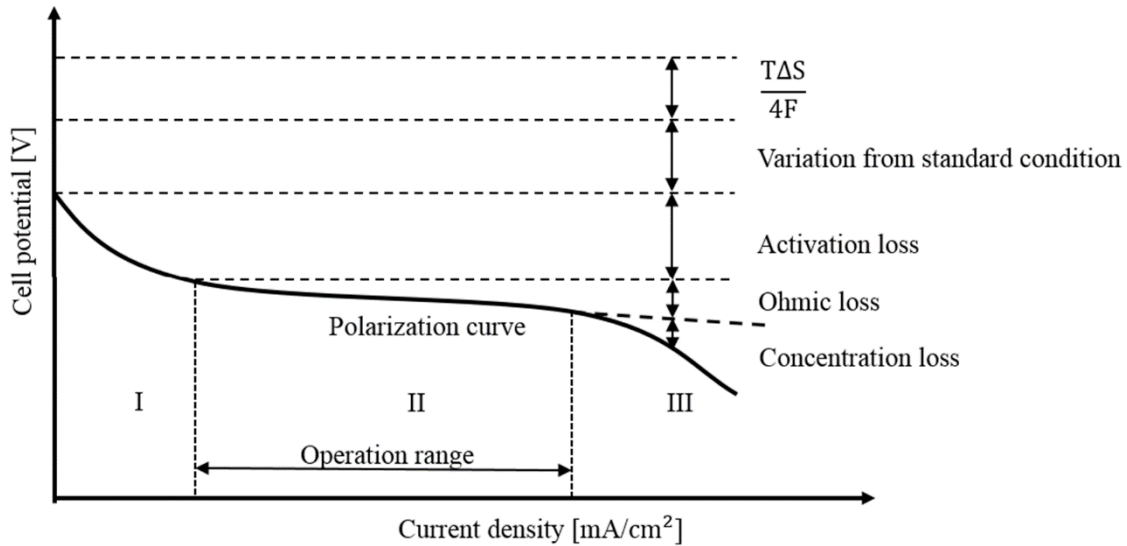
Figure 4 Polarization diagram of PEMFC.

This graph illustrates what the PEMFC stack's output voltage would be:

$$V_{output} = E - V_{act} - V_{ohmic} - V_{conc} \tag{12}$$

1.2 Effects of operating conditions on PEMFC performance

The operating conditions of the PEMFC may have a significant impact on its overall efficiency. Poor working conditions are the primary cause of the PEMFC's performance fluctuations. We'd want to use a variety of operating situations to illustrate this point, including inadequate water management, poor temperature control, gas hunger, fuel contamination, and load cycling.

1.2.1 Insufficient water management

The PEMFC's output efficiency can be significantly impacted by how water is managed there. Water can enter a PEMFC through the humidified reactant gases or it can be produced at the cathode side by electrochemical processes.

Before being supplied to the anode electrode, the reactant gases are pre-humidified. After that, water is diffused through the membrane, ensuring that it has a suitable proton conductivity. Water is also produced on the cathode side by the oxygen reduction process.

Other than water management, nothing in the PEMFC could be more paradoxical. A sound water management plan is essential to maintaining the PEMFC's functionality. On the one hand, without water, protons could not permeate across the polymer membrane from the anode to the cathode side. On the other side, water may obstruct the pores in the GDL or the flow field channels of the bipolar plates, slowing down the processes in the fuel cell. The local reactant shortage in the operating fuel cells might result from this. Furthermore, too much water might lead to a considerably more humid atmosphere. The bipolar plates and GDL in the fuel cell would corrode in this environment with too much water, for example. Particularly, because too much water might produce a corrosive environment, it will hasten the aging of GDL and bipolar plates. It combines the bipolar plates' and GDL's deterioration. Hence, during regular operation, the fuel cell's water management is crucial.

In essence, poor water management might cause membrane drying or flooding on the electrodes.

> *Flooding of electrodes:*

Both the anode and cathode sides of the electrodes might get flooded.

i.   Flooding at the cathode side:

Flooding on the cathode side occurs far more frequently than on the anode side. This is due to the fact that water is created on the cathode side of the fuel cell during the reaction, and that protons traveling from the anode side would likewise draw water molecules from the anode side to the cathode side, resulting in cathode flooding. The water-dragging phenomena in this process are known as electro-osmosis. Mass transit inside the GDL may be hampered by floods on the cathode side. This might make it more difficult for the oxygen to get to the reaction sites. In certain severe circumstances, this blocking of the pores in the GDL might induce local oxygen deficiency. The oxygen would travel in different routes because of the obstruction. As a result, the flow field channels may experience an imbalanced pressure, which would lower the PEMFC stack's efficiency [11]. Under larger current densities, cathode flooding typically occurs. In a particular experiment, He et al. [12] showed that when the cathode is flooded from 1.5 kPa to about 3 kPa, the output voltage of a single cell will fall from 0.9V to 0.3V. Cathode purging is often able to reduce cathode flooding. The GDL in the PEMFC should all have the PTFE coating treatment applied to its surface, as has already been indicated. Hence, the proportion of hydrophobic holes in the GDL is somehow connected to the PEMFC stack's maximum power. The hydrophobic holes are essential for allowing the water created on the cathode to escape while the stack is working at a high current profile.

Also, with the prolonged operation, the extra water in the cathode would cause corrosion on the bipolar plates. The pores of the GDL might be blocked by dissolving or dissolved particles from the corrosion sites on the bipolar plates, and the particles may even permeate into the membrane, reducing the proton conductivity of the membrane.

A PEMFC stack's efficiency may suffer as a result of both of these.

ii.   Flooding at the anode side:

In a PEMFC stack that is working correctly, anode flooding is uncommon. Nonetheless, in some specific circumstances, the anode could experience flooding and have similar effects as the cathode. Typically, while the stack is functioning at a relatively low current density, flooding on the anode side of the fuel cell frequently occurs. Since the low flux of protons moving from the anode to the cathode in the membrane in a low current operating profile, electro-osmosis would not be sufficient to balance the water environment in the anode. This type of anode flooding may occur, particularly if the anode is powered by highly hydrated hydrogen. Incorrect water injection into the anode might also result in anode flooding.

➢ *Membrane dehydration:*

Owing to electro-osmosis in the membrane, dehydration often occurs on the anode side of the fuel cell. Protons may move the water molecules to the opposite side of the membrane, resulting in a discrepancy in the amount of water on the two sides of the membrane. Although reverse diffusion is physically preferred for replenishing lost water, the anode may still get dehydrated while in use, particularly when running at high current densities or receiving fuel that isn't sufficiently humidified [13].

The poor proton conductivity of the membrane might be caused by the membrane's declining water content. As a result, operational efficiency would suffer. Büchi et al. [14] detected a PEMFC in the experiment of during 1200 hours of continuous running with no humidification on the anode side. The current density reduced from 170 to 130 mA/cm^2 at the constant output potential of 0.61V.

The rehydration process on the anode side may be able to restore some efficiency. Yet, prolonged membrane dehydration would lead to a permanent decline in performance. Any membrane that operates in dry circumstances will inevitably develop internal fissures or brittleness. The quantity of gas crossing between the electrodes would undoubtedly rise as the number of fractures grew. The dissolute platinum particles inside the membrane would react with the crossed-over gases, resulting in the formation of pinholes. Additional gas would cross through as a result of these pinholes. This is one of the primary membrane degradation phenomena.

1.2.2 Poor thermal management

The efficiency drops or degradation over a sufficient period of time might be brought on by the PEMFC stacks' inadequate temperature regulation. Under cold temperatures, it might, however, drop significantly [15] [Wang, Y. (2007). Analysis of the key parameters in the cold start of polymer electrolyte fuel cells. Journal of the Electrochemical Society, 154(10), B1041.]. Moreover, performance suffers while operating in environments with high temperatures (>80°C) [16, 17].

➤ *Sub-zero condition:*

The freezing or sub-zero operating situation is the most frequent temperature-related circumstance that might result in an efficiency of drops or degradation in a fuel cell .He et al. [18] presented comparison research examining the influence of several membranes under sub-zero temperatures. The findings demonstrated a substantial correlation between the water content and membrane thickness and the volume change brought on by ice formation. After this freezing test, the Nafion 117 membrane is much thicker than the Nafion 112 membrane for two membranes that were fully hydrated before the sub-zero test. Physically, the sub-zero or fluctuating temperatures near 0 °C might cause fractures to form inside the membrane, increasing the amount of crossover between the electrodes. Pinholes that develop throughout the operation may lead to further membrane breaches and a reduction in fuel cell stack efficiency. Intriguingly, Kim et al. [19].'s research demonstrates that no physical damage could be seen in the membrane or on the catalyst layer during freezing for those cells that were thoroughly dried after the operation.

➤ *Elevated temperature condition:*

For various reasons, the engineers occasionally tended to keep the PEMFC stack operating at higher temperatures (over 100°C) [Yuan, H., Dai, Y., Li, H., & Wang, Y. (2022). Modeling of high-temperature polymer electrolyte membrane fuel cell for reaction spatial variation. International Journal of Heat and Mass Transfer, 195, 123209.]. Secondly, at higher temperatures, electrochemical processes would have faster reaction kinetics. Moreover, a greater temperature could increase the PEMFC's tolerance for fuel contaminants. Therefore,

in this situation, the effects of Carbon monoxide poisoning may be lessened, which may increase the PEMFC stack's durability when supplied with lower-quality hydrogen.

Yet, the increased temperature may be to blame for the fuel cell's performance drop or long-term degradation. The fact that the catalyst layers might degrade more quickly at an increased temperature is what matters most in this situation. Under a high-temperature setting at the cathode side, the platinum particles would become more potentially unstable. The nano platinum particles would tend to group in this manner and have a lower chemical potential. This aggregation process, also known as the Ostwald ripening phenomenon, may result in the loss of ECSA and a possible decline over time.

Moreover, the undesired response on the cathode side can be brought on by the higher temperature. The high temperature and voltage on the cathode side would cause the oxygen molecules to divide into two oxygen atoms. In this manner, the carbon substrate might interact with the atoms inside the cell to produce CO_2 or CO. This implies that the increased temperature may affect the carbon structure in the GDL or perhaps speed up carbon corrosion in the catalytic layer.

In particular, while fuel is supplied with improperly pre-humidified fuels, the increased temperature operating circumstances may result in a decrease in the proton conductivity. The membrane's ohmic losses may rise due to the decreased proton conductivity, which would lower performance across the board.

1.2.3 Reactant starvation

Reactant starvation in a fuel cell refers to a lack of oxygen or fuel. This would always result in sub-stoichiometric functioning circumstances for fuel cell. Gas starvation may result in a possible drop in the efficiency of fuel cells. Gas starvation in a fuel cell can frequently result in undesirable events occurring on both electrodes. Whenever supplied with oxygen, fuel cell must produce water on the cathode side. Nonetheless, under gas deprivation conditions, this reaction's cathode side emission of hydrogen might be seen:

$$2H^+_{(aq)} + 2e^- \rightarrow H_{2_{(g)}} \tag{13}$$

When the oxygen might be emitted from the anode side:

$$2H_2O_{(aq)} \rightarrow O_{2_{(g)}} + 4H^+_{(aq)} + 4e^- \tag{14}$$

In some circumstances, the Carbon dioxide might also be recognized, and the cathode side could experience the below reactions:

$$C_{(s)} + 2H_2O_{(aq)} \rightarrow CO_{2_{(g)}} + 4H^+_{(aq)} + 4e^- \tag{15}$$
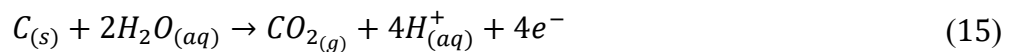
These various reactions show how gas shortage may change the composition of the gas through each electrode, producing hydrogen on the cathode side and oxygen on the anode side. In addition to this occurrence of the reactant gases reversing, the carbon support is oxidized and destroyed because of gas starvation at the anode side, which may cause the electrodes to degrade over time.

Cold starts or inadequate water management are the usual culprits for gas starvation. In either scenario, the pores in the layer of gas diffusion might be blocked by water or ice,

preventing reactant gases from reaching the reaction sites. The uneven flow field channel design or an abrupt increase in load might both result in gas starvation and worse fuel cell efficiency.

1.2.4 Contamination

A reduction in the efficiency of fuel cells might be brought on by contamination. Often, the term "contamination" refers to contaminants that enter the fuel cell together with the fuels. Contaminants may occasionally be shown to have originated from cell components. After all, catalyst particles, metallic ions, CO, NO_x, and SO_2 are frequently found among the contamination's impurities. The pollution could have a significant impact on how well the membrane and electrodes work.

Because of the contamination of the membrane by pollutants like ammonium or alkaline metal ions, the protons may not be able to connect to the PFSA end groups. Due to the higher ohmic resistance, this event may significantly reduce the fuel cell's efficiency. Because of the limited electro-osmosis inside the membrane in some severe situations, contamination may result in dehydration at the cathode side, which would impair output performance and exchange current density [20].

Furthermore, carbon monoxide on the anode side is frequently the source of contamination for electrodes. The term "CO poisoning" refers to this contamination mechanism. If the hydrogen is generated by reforming the hydrocarbons, the CO is first delivered to the cell together with the hydrogen. The platinum particles on the catalyst layers

may get bonded to CO molecules, severely reducing the ECSA, and this is the mechanism of CO poisoning. Because of the substantial CO coverage in this reaction, the hydrogen is prevented from reaching the covered reaction sites on the catalyst layers, which might lower output performance. Carbon monoxide poisoning, therefore, is treatable and reversible. By merely blowing some air into the anode side, the connected CO molecules would be burnt and converted to Carbon dioxide with the airflow, reducing the impact of CO poisoning [21].

1.2.5 Voltage cycling

The platinum might clump together on the catalyst layer as a result of voltage cycling, which would lower the ECSA. ECSA shrinkage is the name given to this occurrence. In actuality, the number of possible cycling affects and lowers the ECSA in the fuel cell at the cathode side during the ECSA shrinking [22]. The rate of ECSA degradation would increase with the number of possible cycles. Furthermore, during typical processes (1V), the peak value of the potential cycle also has a significant impact on the aging of the ECSA. The ECSA would degrade more quickly the greater the possible cycles.

Since platinum particles could only dissolve at higher potentials, the load cycling in the PEMFC stack could only have an impact on the catalyst layer on the cathode side [23]. Compared to the potential on the anode side, the potential at the membrane and cathode contact is significantly greater. Hence, the cathode catalyst layer is far more susceptible to load cycling than the one on the anode side.

It's actually intriguing that during cycling, greater cathode potentials (>1V) might potentially result in the formation of a platinum oxide layer on the platinum particles' interface. This oxide layer, which was created at a greater potential, may then stop the platinum particles from eroding into the membrane. PtO covers surfaces of platinum particles at a rate that is proportional to potential; a greater potential would result in a quicker covering rate of PtO.

This ECSA-related degradation is especially shown in [24]. For further details, we gladly suggest the readers to [24]. We only consider the formation of the PtO monolayer and the dissolution of platinum particles as they are affected by changes in potential. The possible cycling might also result in carbon corrosion on the catalyst layer or the GDL in addition to the ECSA degradation.

Chapter 2: PEMFC degradation

The PEMFC components might decline or stop working throughout normal system operation because they are vulnerable to the aging phenomenon, which results in PEMFC degradation or failure. Thus, it is crucial to carefully and in-depth study and comprehend the causes of degradation. In actuality, it is impossible to simply isolate the degradation processes of the various fuel cell components because they are typically impacted by one another. Nonetheless, it is preferable to show the various methods on each component separately in order to make it obvious and legible for the readers.

2.1 Degradation mechanism

Several degradation modes may occur during fuel cell operation [25]. Much degradation typically occurs in the GDL, catalyst layer, and polymer membrane. Carbon corrosion is the main degradative process in the GDL. The GDL is often constructed of fabric or carbon paper. High humidity and/or potential (load) cycling of the PEMFC is the two main causes of carbon corrosion, respectively [26, 27]. In addition, platinum (the catalyst) rearrangement (sintering) in the catalyst layer is frequently regarded as a crucial element affecting the long-term efficiency of PEMFC. The platinum particles in electrodes are affixed to the interface of the carbon substrate or support, making them subject to degradation of the carbon structure. Moreover, platinum particle sintering can frequently be seen while running in load-cycling or high-humidity or high-temperature conditions [24, 28]. It is thought that the hydroxyl (OH) and hydroperoxyl (OOH) radicals' chemical assaults on the

polymer membrane are what first reason for the membrane to degrade. Hydrogen peroxide (H_2O_2), which is produced as a result of fuel pollution or gas crossing, is the source of these radicals. The breakdown of polymer structure and alteration of membrane characteristics are caused by chemical assault and temporary operational conditions [29-32]. Table 1 summarizes the significant processes and reasons for degradation.

Table 1 The causes and effects of PEMFC degradation.

	Carbon Corrosion	Platinum loss	Membrane degradation	Structural stress
Electrical	353	0.75	0.75	0.9
Data2	333	0.75	0.25	0.34
Data3	293	0.99	0.99	0.74

2.2 Component degradation

2.2.1 Membrane degradation

In the majority of literature evaluations, the three types of membrane degradation-chemical, mechanical, and thermal-could be distinguished. A somewhat different classification-chemical deterioration, mechanical degradation, and crossover-related damage-was proposed by Gittleman et al. in [4]. These three factors would be used in this thesis study to explain how the membrane degrades.

1) Chemical degradation

It is acknowledged that one of the main factors limiting the polymer membrane's lifespan is chemical degradation. The membrane thinning and the release of HF, CO_2, and H_2SO_4 during the process are indicators of the chemical degradation of the membrane. Decreased membrane thickness starts a gas crossover and makes the membrane more brittle

mechanically. Fundamentally, it is believed that the toxicity of the contaminated species and the activities of species of aggressive radicals that are created during the process of the stack is to blame.

The weak connections in the polymer structure might be attacked by the radicals. Due to their excellent chemical stability, perfluorocarbon-sulfonic acid ionomers (PSA) are a necessary component of the membrane. In a fuel cell, it has to be both chemically and mechanically stable. Unfortunately, perfluorinated compounds are not inert while the stack is in use over an extended period. The membrane decomposes as a result of the chemical degradation, which is brought on by radical species attacking the polymer directly. The main species responsible for assaults on the membrane are reactive species like hydroxyl (OH), hydroperoxyl radicals (OOH), and hydrogen peroxide (H_2O_2). The problem of radical attacks is covered in [4, 29, 32-34].

An unstable membrane state is imposed by the oxidative environment on the cathode side and the reductive environment on the anode electrode, which might hasten the chemical degradation of the membrane. The PEMFC's operation at relatively low humidity and greater potential may further speed up chemical degradation.

Additionally, poisonous species hasten the chemical degradation of the membrane. These compounds, which also are hypothesized to be generated by nearby metallic pipes or apparatus, include the cations Fe^{3+}, Cu^{2+}, and others. The ability of these cations to connect to the end groups in the polymer electrolyte would minimize the space available in the membrane for protons to attach, which would result in a reduction in the conductivity of the

membrane and, consequently, in the output voltage of the entire stack. This makes the membrane especially vulnerable to the existence of these cations.

2)   Mechanical degradation

Typically, cyclic working conditions are what lead to mechanical degradation. The membrane would be susceptible to mechanical degradation, in this case, known as hydrothermal fatigue, whenever it expands and contracts with changes in humidity or temperature. The membrane would develop tiny pinholes as a result of this type of degradation, which would also enhance the rate at which gases traverse the membrane from either side.

Moreover, the Xo plane of the membrane would experience local tension as a result of the catalyst particle buildup. The sources [27, 35] go into great detail about it. In reality, the Pt particles would tend to diffuse through the membrane even under normal operating conditions. Since the included dissolving reaction is encouraged at a higher potential, the Pt particles on the cathode side would particularly dissolve into the membrane. These dissolved platinum ions have the potential to be decreased by the hydrogen crossed over from the anode side and can build up in a specific area of the membrane (the Xo plane) where the concentration ratio of the crossed-over hydrogen or oxygen is preferred.

3)   Crossover related damage

The crossover in a PEMFC refers to the potential for hydrogen or oxygen to pass across the membrane and reach the reaction sites on the opposite electrode. The reactant gases that were crossed over might interact with one another inside the membrane or on the electrodes.

The reactions that took place on electrodes with the crossover gases included were deemed chemical combustion reactions instead of electrochemical reactions. As a result, it is thought that this portion of the reactants given to the fuel cell was squandered during the crossover. So, a PEMFC would only be regarded as an energy converter if the electrons it is driving are coming from an external circuit and aren't just being squandered on the electrodes.

In addition, the membrane's crossing of the reactant gases would result in the gases inside the membrane interacting on the surface of the precipitated platinum particles. The membrane would be significantly damaged by this combustion event, leading to increased membrane crossing. Numerous studies [36, 37] have documented the exponentially rising profile of membrane aging-related crossover in the literature.

2.2.2 GDL degradation

The GDL degradation would affect the fuel cell stack efficiency throughout aging and operating time, much as other degradation components. The GDL layer is often formed of carbon paper or cloth, which is heavily squeezed between the bipolar plates and MEA within every cell, as has been previously discussed. It is a crucial part of the PEMFC because it acts as a conduit for the diffusion of the reactants from the bipolar plates to the reaction sites while also releasing the water produced during the reaction if the droplets would otherwise obstruct the pores through which the reactant gases pass.

The GDL degradation will be specifically shown in this thesis project from the viewpoints of chemical and physical degradation:

1)   Chemical degradation

The GDL's chemical composition would alter over time. Particularly, the hydrophobicity of the GDL would diminish with time. During fabrication, the GDL is typically treated with a PTFE coating. Teflon pans, often known as non-stick pans, are frequently coated with PTFE. The benefits of high hydrophobicity, high operating temperature, an exceptionally low coefficient of friction, acceptable abrasion resistance, and strong chemical resistance would be conferred onto the GDL by this coating.

Although, the change from hydrophobic to hydrophilic always happens gradually. According to the aging experiments described by [33], the hydrophobicity would rise with operating temperature while falling with time. The carbon cloth's binding forces weaken when the PTFE coating breaks from it, and this can lead to the formation of hydrophilic surfaces on the GDL. Because there are more hydrophilic surfaces, throughout the long-term operation, the reactant gases would be prevented from reaching the reaction sites by the water droplets.

2)   Physical degradation

Physical qualities are always thought to alter as a result of physical deterioration. This is mostly caused by carbon corrosions that mechanically modify the GDL's structural completeness and also result in an imbalanced force distribution from the membrane or the bipolar plate.

Carbon corrosion remains an important factor in the GDL's physical degradation. On the cathode side, where the potential is substantially greater than the equilibrium potential for the carbon oxidation process (0.207V), carbon is considered to be thermodynamically

unstable [38]. Most precisely, carbon corrosion would frequently happen during start-stop operations while air is supplied on the anode side of the fuel cell. This would potentially elevate the carbon corrosion rate on the cathode side of the fuel cell, which would then rise [39-41].

Furthermore, carbon corrosion would be brought on by fuel starvation [42]. The GDL layer may fracture or separate due to carbon corrosion, which might also result in a change in the GDL's mechanical structure and an imbalanced distribution of force from the membrane or the bipolar plate. The electric or thermal resistance of the GDL layer would alter as a result of all of these scenarios.

2.2.3 Catalyst layer degradation

The catalyst is mostly composed of nano platinum particles with sizes between 2 and 5 nm. If the characteristics of those tiny particles changed, it would have a significant impact on the PEMFC stack's efficiency. Based on the [43], dissolution, oxidation, or agglomeration on the anode side would rarely have an impact on the platinum particles. Unfortunately, because of the higher potential environment, the platinum particles on the cathode side are not entirely stable. The platinum particles would be oxidized to platinum ions and subsequently dissolved into the membrane as a result of this increased potential producing an oxidative environment. As a consequence, the catalyst layer's ECSA would gradually decline. The majority of the time, it can be caused by cyclical operating conditions, such as a potential cycling or temperature cycling operation profile.

Generally, these three processes are considered to be catalyst degradation:

I.   Platinum particles diffuse through the ionomer, dissolve and re-deposit on other platinum particles to make bigger particles (Ostwald ripening), then diffuse through the membrane to form the platinum band (Xo plane).

II.   Producing oxidative compounds that would lead to membrane breakdown. The radical's hydroxyl (OH), hydroperoxyl (OOH), and hydrogen peroxide (H_2O_2) would always be present in these species (usually occurred on the platinum particles precipitated in the membrane).

III.   Adsorption of contaminants from the air, reactants, or other damaged materials that may be reversible or irreversible.

To demonstrate the Ostwald ripening, that contributes to catalyst degradation and results in ECSA reduction, in this thesis project, we will be more explicit.

A phenomenon known as the Ostwald ripening, which may be seen in solid (or liquid) solutions, shows how an inhomogeneous structure changes over time. Wilhelm Ostwald [44] published the first description of the phenomena in 1896. Energy-related variables will cause major precipitates to expand whenever a phase precipitates out of a solid, taking material from smaller precipitates, which shrink. Another way to say, bigger particles tend to grow in size while smaller ones prefer to shrink in an inhomogeneous environment. *Figure 5* depicts this procedure.
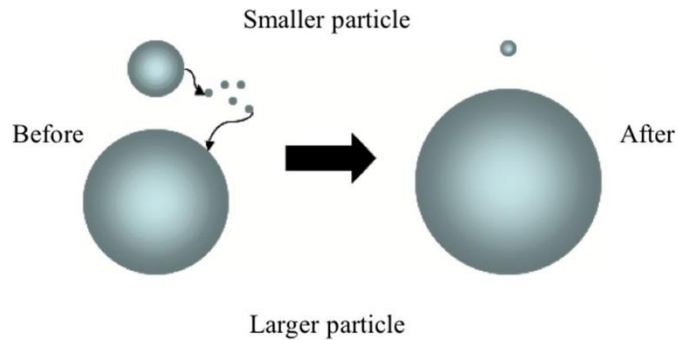
Figure 5 Ostwald ripening processes [44].

Due to the larger particles being much more energetically stable than smaller particles, this thermodynamically driven spontaneous process happens. This is because the internal pressure is inversely correlated with the particle's radius. It results from the fact that molecules on a particle's surface are less energetically stable than those that are previously arranged and tightly packed within. Large particles would have a reduced surface energy because of their smaller surface-to-volume ratio, which leads to a lower energy state. The molecules on the surface of a tiny (energetically inadequate) particle will typically tend to detach, diffuse through the solution, and then adhere to the surface of a bigger particle as all chemical systems attempt to reduce their total energy. As a result, although larger particles continue to expand, the number of smaller particles continues to decline.

This type of phenomenon would occur with platinum particles in the fuel cell environment, particularly if the particles were inside the membrane or on the surface of the cathode side catalyst layer. This is taking place as a result of the platinum particles being excited to an unstable condition by the greater potential on the cathode side; once the potential is favorable, they prefer to disintegrate from the reaction site. Because of the

37

oxidative interaction with the H$_2$ crossed over from the anode side, the platinum particles in the membrane have a tendency to precipitate and aggregate.

On the one hand, the ECSA would decrease over time as the size of the platinum particles increased for the Ostwald ripening on the cathode side. In contrast, the membrane's Ostwald ripening would result in the precipitation of platinum there. This would cause the membrane to mechanically degrade, which would lead to tiny pinholes and speed up the crossing of gases from both sides of the membrane.

2.2.4 Degradation on bipolar plates, gaskets, and others

There are just two studies that discuss the degradation of bipolar plates in the research [9, 43]. These two publications reveal three processes at play:

1.   Long-term corrosion brought on by the bipolar plates' acidic environment would result in the formation of undesired cations, which would negatively affect the membrane and catalyst layers' resilience;

2.   Long-term corrosion would produce a layer of resistance on the surface, increasing the ohmic contact resistance;

3.   On the plates, deformations or cracks would occur. They are a result of cyclical operating circumstances like temperature cycling that would lead to an uneven distribution of temperature in the bipolar plates.

The stacks are crushed in addition to the bipolar plates by the gaskets and seals. It is currently uncertain how these components will age. The causes and consequences of a few things are shown in [9]. The compression force that the gaskets would give can be impacted

by the temperature stress and the acidic environment. The materials could occasionally dissolve or dissolute in this acidic medium. The hydrophobicity of the GDL may be impacted by their movement and precipitation in the electrodes, and they may also contaminate the membrane and catalysts. In addition, with the prolonged operation, breakdown products might be detected in the MEA. No literature has yet suggested a degradation model for this component.

2.3 Prognostics of PEMFC

Prognostics, as a whole, refers to the assessment of the degree of a system's deviation or degradation from its anticipated normal state of operation to forecast the future efficiency of one or more components [45]. The engineer would know, thanks to predicting the performance, whenever the system or a component will stop serving its intended purpose. In many literary works, the prognostics-which includes the remaining usable life (RUL) forecast-are always tied to the performance projection. We discuss the performance prediction of PEMFC in this research thesis. It refers to the evaluation of the gathered historical data to estimate or forecast the long-term performance fluctuation of the fuel cell stack.

Prognostic methods in the field of engineering control may essentially be categorized into three groups: data-driven, model-based, and hybrid methods. Articles on these 3 groups have always been accessible through literature.

2.3.1 Data driven methods

The historical data that is tracked and collected forms the foundation of data-driven techniques. The engineer would have to remove the degradation or behavior aspects from the gathered data using data-driven methodologies. An RUL or performance variation can be anticipated once the historical data has been trained. In actuality, data-driven methodologies are the focus of the majority of prognostics research studies. There are papers connected to Bayesian probabilistic [46-49], neural networks [50-54], Kalman filter [55], or just straightforward regression methods [56]. These methods are often calculus-friendly, relatively easy to apply, and do not call for analysis methods of system degradation. Unfortunately, they occasionally had low prediction performance, which caused the models' output to differ from the system's real behavior. In order to achieve a compromise between application and precision, data-driven techniques are used.

2.3.2 Model based methods

The model-based techniques call for the creation of a physical dynamic model that captures the system's behavior and includes degradation phenomena (primarily the phenomenon of wear, corrosion, or fatigue) whose evolution might be studied [57-62].

Commonly, these sorts of procedures could produce prognosis outcomes that are more precise than those from the other two ways. They do, though, have several significant flaws. On the one hand, it is challenging to construct the physical dynamic model since it is typically challenging to analytically characterize the degradation processes. The physical degradation approach, on the other hand, is typically difficult to execute in in-situ prognostic

situations, where the quick and accurate prognostic model is always preferred. Furthermore, the physical dynamic model of one system or component may not always be generalizable to others, making it challenging to apply the degradation model to other systems or components. As a result, the application space for model-based techniques is rather constrained.

2.3.3 Hybrid methods

Hybrid prognostic techniques are often a type of strategy that combines model-based techniques with data-driven techniques. During the prognostic process, data and physical model information from a system are exchanged. The series configuration and the parallel configuration are the two main types of hybrid techniques.

When compared to some of the unobservable characteristics in the physical dynamic model, which are calculated or estimated by various data-driven approaches, the series configuration is often recognized as a model-based prognostic approach. This style of predictive methodology is covered in [63].

A "parallel configuration" combines a physical model's output with a data-driven approach's output to supply an overall outcome. The data fusion strategy, in which the output results of two models are combined to get a global forecast outcome, and this sort of method are fairly comparable. Several publications have been discussing this subject area in the literature [64, 65].

2.4 Data-driven method

2.4.1 Artificial Neural Networks

Artificial Neural Networks (ANNs) are nonlinear mapping mechanisms designed to mimic the operations of the human brain. They consist of a set number of neurons, which are central processing units, coupled by connecting weights, which are unidirectional signal channels. Given that they can manage the most complicated scenarios that are not adequately stated for carrying out deterministic algorithms, neural networks are a machine learning technique (ML) that provides a significant and practical replacement for traditional approaches [66]. According to its fundamental characteristic that enables the approximation of any continuous non-linear relationship using a neural network with appropriate design and weight variables, artificial neural networks offer an excellent mathematical mechanism to handle nonlinear challenges [67]. The artificial neural networks also possess a number of desirable qualities, including the capacity for internal mapping of the functional relationships that represent the process, the capacity for learning functional dependencies of data, the capacity for high computation rates, the capacity for large input error tolerance, the capacity for noise filtering, and the capacity for handling correlations [66-68]. Across a wide range of industries, such aerospace, manufacturing, engineering, military, health care, the oil and gas sector, finance, securities, transportation, telecommunications, and environment, neural networks have been used to solve modeling and classifying issues [67-69].

The explosive expansion of what has been dubbed "Deep Learning" is one of the most astonishing phenomena in the field of machine learning. Neural network research and application have undergone a revolution as a result of deep learning. Any multilayer artificial neural network could be a deep learning instance because deep learning is a cluster based on various ANN architectures. We refer to these networks as deep neural networks (DNNs) because every layer can solve complex functions like representation and abstraction that make sense of sound, images, and text. As neural networks feature several (deep) layers that enable learning, we coined the term "deep learning" to refer to the number of layers that are employed in the network. In terms of feature learning, model building, and model training, deep learning techniques have numerous benefits over classical ML [70]. Deep learning, as opposed to manually designing the most effective data representation with domain expertise, permits for the automatic data processing through very nonlinear and complex abstraction of characteristics over a cascade of numerous layers to find the complex fundamental patterns. The more the model learns, the better it gets at solving complicated issues despite the fact that it uses a wide variety of unstructured, interrelated data. Although there are many distinct forms of learning in machine learning, they may typically be categorized into four classes based on their intended use:

I.   Supervised Learning: Whenever the actual result with information is present, this strategy is utilized, where the learning algorithm receives a set of inputs in addition to the intended results. Its result might be actual value or discrete/categorical (e.g., a certain color, an image of an animal, a vehicle model, etc.). By comparing the actual output with the present output to identify faults, the learning process updates the model as necessary by

using various techniques including regression and categorization [71]. All of the models that are suggested in our thesis fall under this heading.

II. Unsupervised Learning: This technique allows for the extraction of all the useful data from a particular database for further processing and analysis without the requirement of ground truth data or expert supervision (labels). Such a strategy can go in one of 2 ways: either by utilizing cluster analysis to detect intriguing patterns, or by employing association evaluation to identify some extremely valuable associations between the variables of a huge database [72].

III. Semi-supervised Learning: This strategy is employed anytime there is a mix of labeled and unlabeled training data, often a small quantity of labeled data and a big volume of unlabeled data due to the cheaper cost of unlabeled data relative to labeled data [71]. The same applications of supervised learning may be utilized with this sort of learning, and it is also feasible to combine it with supervised learning by using the unsupervised methodology for label prediction. This approach is especially suitable for picture collections when not every image is typically tagged [72].

IV. Reinforcement Learning: The reinforcement learning framework is built on an agent that interacts with its environment to learn, and the agent must decide which behaviors to do in order to enhance the expected reward over a certain duration. The objective of this sort of learning is to find the best policy since it will enable the agent to hit the target much faster. The agent, or learner, the environment, and the agent's behaviors are the three major elements in this sort of learning [72]. Reward-based learning is tailored for particular issues including gaming, robotics, and navigation. Moreover, it uses either one of

the following ways to solve the reinforcement tasks: value function methods, policy search methods, or both [73].

According to the ANN concept, a wide variety of structures were created, each with a unique architecture style, data processing (input-output), and learning methodology. Amongst numerous, one may choose the most well-liked methods, which served as the cornerstones of deep learning, the new cluster of ANNs. Some methods include:

    i.   Multilayer Perceptron Networks (MLP).

    ii.   Convolutional Neural Networks (CNN).

    iii.   Recurrent Neural Networks (RNN).

Deep learning approaches have demonstrated improved performance when it comes to tackling complicated prognostic problems with a variety of systems whose degradation processes are challenging to connect using alternative methodology. These architectures stack numerous layers of information processing modules in hierarchical structures to model high level representations of information and estimation/classify patterns [74]. Also, it was used to solve numbers of issues in manufacturing and industrial operations, and its efficiency and notable outcomes in the use of predictive health management have beyond expectations [75]. For various systems, including high-speed CNC machines, induction motors, gearboxes, air compressors, and aviation engines, to mention a few, in particular problem detection, diagnosis, and RUL estimation. An overview of the aforementioned architectures will be provided in the following subsections.

2.4.2 Multilayer Perceptron Networks (MLP)

Given that it serves as the foundation for all neural networks, MLP is one of the most frequently utilized neural networks [76]. As we will see, it is commonly utilized as a stand-alone model [77] or as the last layers of more sophisticated and complicated neural networks, such as CNNs or RNNs. The network's efficiency (Result) depends solely on the current input instance, making MLP a feed forward artificial neural network design [78]. By way of explanation, this MLP is made up of interconnected neurons that transmit information among themselves, much like the human brain [76]. Every level is linked to the contiguous layer by a set of connections, each connection being equipped with a weight. It is divided into three main parts: an input layer, an [67] intermediate layer (one or more), and an output layer. The input layer, one hidden layer, and the output layer are the three layers that make up the construction of an MLP in
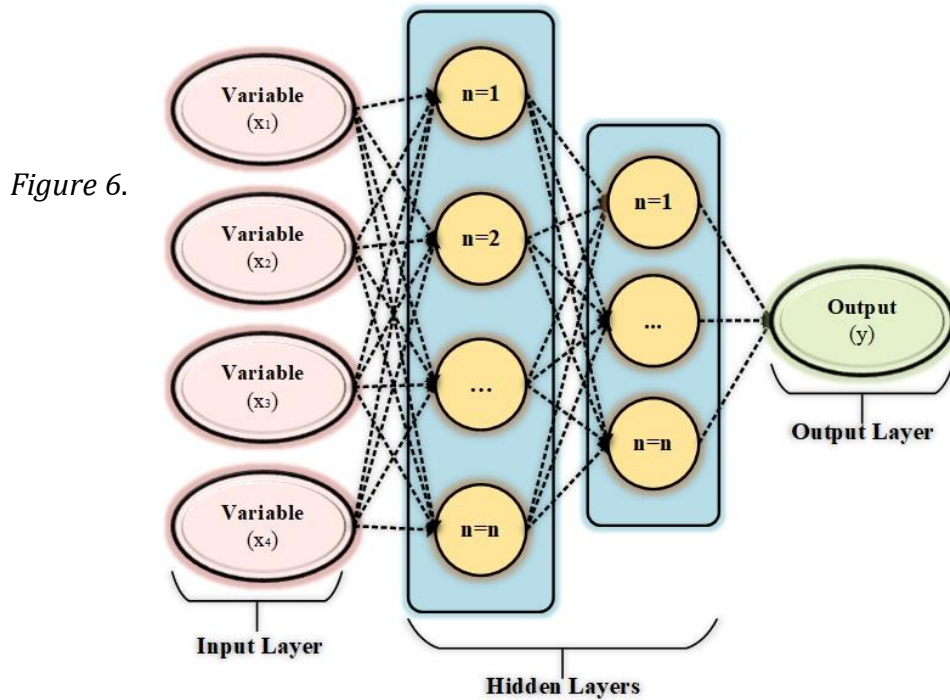

Figure 6.

Figure 6 The structure of MLP Method.

The input layer, represented by $\boldsymbol{x} \in R^k$, is immediately transferred to the first hidden layer, represented by $\boldsymbol{h} \in R^n$, before creating the output, represented by $\boldsymbol{y_0} \in R^0$. The output from every layer may then be determined using the formula below:

$$\boldsymbol{h} = \varphi^{(1)}(\boldsymbol{W_1}x + b_1) \tag{16}$$

$$\boldsymbol{y_0} = \varphi^{(0)}(\boldsymbol{W_0}h + b_0), \tag{17}$$

In the above equations, $\boldsymbol{W_1} \in R^{n \times k}$, $\boldsymbol{W_0} \in R^{0 \times n}$, $b_1 \in R^n$, and $b_0 \in R^0$ are the weights and bias of every layer. Also, φ shows the activation function.

Mathematical functions known as **activation functions** define the nonlinear relationships among both input and output. By calculating the weighted sum and adding bias to it [79], which will add non-linearity to the neuron's output, the activation function has a role in every neuron, calculating whether to consider this neuron as activated "fired" or not. This depends on whether or not each neuron's input is noticeable for the predictive model. Given that nonlinearity characterizes the majority of real-world data, this feature is crucial. The activation functions may be as simple as a step function, which regulates the neuron output by turning it on and off by predetermined guidelines or bounds. Nevertheless, they might also be non-linear activation functions, which would allow the network to handle more complicated data, learn and calculate virtually any data-related attribute, and provide precise predictions [79].

47

There are several well-known and popular activation functions, including:

I. One of the most common activation functions is the sigmoid or logistic function, and it takes the following form.

$$sigmoid\ (x) = \frac{1}{1 + e^{-x}} \tag{18}$$

It converts (normalizes) actual input quantities inside the R domain into outputs that fall within a range (0, 1).

II. A further activation function, the hyperbolic tangent function (*tanh*), is fairly similar to the preceding one but takes the general formula:

$$tanh\ (x) = \frac{1 - e^{-2x}}{1 + e^{-2x}} \tag{19}$$

Its output ranges between 0 and 1 and it is zero-centered, which is why it is frequently chosen over the sigmoid function.

III. Rectified Linear units (*ReLu*): This is the most significant and well-known activation function, which converts real input values R so that the positive values grow linearly while the negative values are transformed to zero:

$$ReLu(x) = \max (0, x) \tag{20}$$

MLP is frequently used with supervised learning models, which train their networks using the back propagation approach. The discrepancy between the outputs and the known predicted results is always represented as an error during training. The cost function is the function that measures this mistake. In order to maximize the correlation between the model and the system it seeks to represent, supervised learning aims to minimize this function [80]. To find the minimal value of the cost function within the weight space, the backpropagation

process relies on the gradient descent approach (or other methods with the same purpose). The weights that succeed in achieving this goal will be regarded as offering the best answer to the current learning conundrum. In order to calculate the derivative of the cost function with respect to the network weights, the gradient descent algorithm does as follow:

$$\frac{\partial Error}{\partial W_1} = \frac{\partial Error}{\partial y_0} \frac{\partial y_0}{\partial W_0} \frac{\partial W_0}{\partial h} \frac{\partial h}{\partial W_1}, \tag{21}$$

In which the cost function's measurement of the mistake is denoted by the word Error. In other words, the idea is straightforward: alter the network's weights and biases to obtain the required output at the output layer. Check [80] for further information on the backpropagation algorithm.

In a variety of industries, including Handwriting Recognition [81], Classification of Healthcare Data [82], Index of Industrial Production [83], and Stock Market Analysis [84], to mention a few, MLP has been employed. MLP has demonstrated great effectiveness in PHM applications, and a variety of methodologies have been put forth. For example, Huang et al. [53] suggested an integrated methodology for examining the whole life cycle of ball bearings. The remaining useful life has been estimated using NN and the weight utilization to failure times after the minimum quantization error has been utilized as a degradation indicator and the degradation period, which is characterized by the fluctuating signal that rises from the start of the defect until the failure of the component, has been monitored. A method to determine the health of a lithium-ion battery utilizing an MLP network was reported by Kim et al. [85]. The MLP network was used by Jedlinski et al. [86] to assess the technical state of a gearbox and to identify the defect as soon as feasible. The MLP method was used by Hu et

al. [87] to diagnose the position and quantity of mass imbalance on aircraft engines, and the outcomes were preferable to those of previous approaches. By exploiting the characteristics of vibration signals in time-domain for bearings in both normal and faulty instances, Almeidaet al. [88] suggested an architecture based on MLP network to perform the fundamental classification task in addition to the fault diagnosis. Geramifard et al. [89], MLP.'s network was utilized to track and forecast a cutter's health, especially the wearing state in terms of the characteristics or collected data. In order to offer a diagnostic method for defect diagnosis and classification in a real gas turbine, Loboda et al. [90] used the MLP. In order to present an intelligent approach that utilizes the strengths of both frequency domain analysis and time scale, Zolfaghari et al. [91] integrated the wavelet analysis and the MLP network to enable autonomous detection of defect severity during the course of a motor. For the purpose of identifying various faults in the gearbox, Heidari et al. [92] suggested a method that combines the MLP, wavelet support vector machine, and continuous wavelet.

2.4.3 Recurrent Neural Networks (RNN)

RNNs are a significant and well-known type of artificial neural network topologies and one of the most often used sequential modeling methods [93]. RNNs are designed to detect the features of consecutive data and utilize trends and patterns to anticipate the following likely situation. RNNs are distinct from the current feedforward neural network paradigms in that they include an internal memory that enables them to recall prior knowledge and interpret current events appropriately [94]. While RNNs, where the word "recurrent" is employed, execute the same procedure for every sequence item, with the

performance depending on the previous computations, classic neural networks are thought to treat all inputs and outputs as being independent of one another. As shown in *Figure 7*, RNN works on the principle of preserving a particular layer's output and feeding it back into the input to forecast the layer's output.
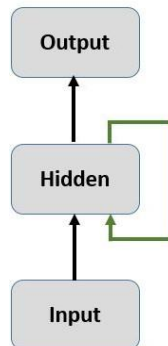

Figure 7 The RNN Concept.

The several input and output relations are reflected by the several structures found in RNNs. Five distinct types of input and output interactions are depicted in *Figure 8*. The three primary types are as follows [94]:

1.   Many-to-one: Whenever the result is a vector with a fixed dimension but the incoming data is a sequence. The sentiment classification serves as a typical instance of a many-to-one algorithm, with a text-based sequence serving as the input and a specific label, such as positive or negative, serving as the result.

2.   One-to-Many: If the input is not a sequence but the result is. This group includes activities that need the input of a picture and the output of a phrase of words.

3.   Many-to-Many: If the input and output are both series and whether or not they are synchronized, this classification may also be separated into subgroups. A synchronized

many-to-many job is an instance of the video classification problem. Whilst the illustration of the unsynchronized many-to-many is language translation.
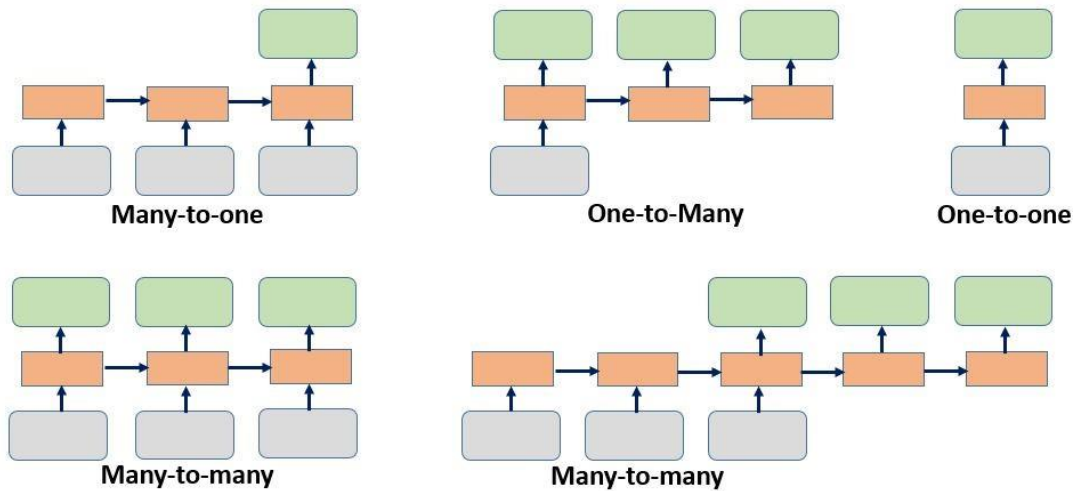

Figure 8 The relationship structures of input and output data [94].

Despite the RNNs' excellent performance in a variety of domains, these networks have several drawbacks, such as the inability to take future contributions to the present state into account. It was for this cause that the bidirectional recurrent neural network, an enhanced version of the RNN, was developed [95]. In this network, input data from the past and future of the current timeline are used simultaneously to determine the same output, with the first direction representing forward states and the second representing backward states, as illustrated in *Figure 9*.
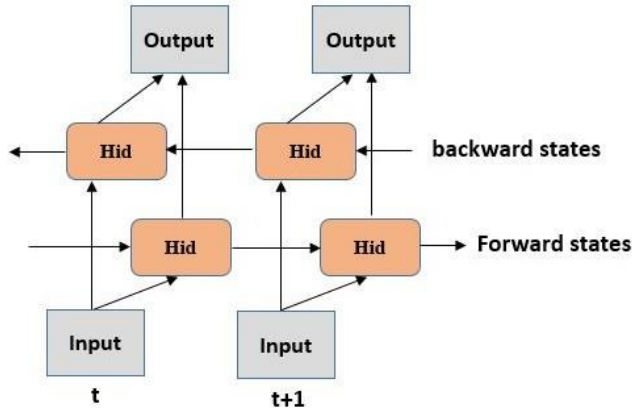
Figure 9 The bidirectional recurrent neural networks [95].

Moreover, the disappearing and inflating gradients are two other major issues that the RNNs face. While the weight matrices are modified utilizing gradient during training (learning), the RNNs generally employ backpropagation. As mentioned earlier, gradients are calculated throughout the backpropagation process by continuously multiplying derivatives, and there is a good chance that these derivative values will get smaller as we move through the network. As a consequence, the gradient will get smaller and smaller until it reaches the "vanish" stage, also known as the "vanishing gradient problem" [93]. Whenever the gradient is very modest, changing the RNN variables (weights and biases) is insignificant, which indicates that no actual learning is done. Gradients provide information that is employed in updating the RNN variables. Particularly, the preliminary layers' variables (weights and biases) won't be updated efficiently between training sessions (as the gradient value is vanishing), which could result in the entire network being completely inaccurate [93, 94]. These preliminary layers are crucial for identifying the essential parts of the input data. On the other hand, the exploding gradients occurred when the big incorrect gradients accumulated, leading to exceptionally massive modifications to the neural network model's

weights throughout the training. Whenever the modifications are tiny but regulated the training process functions flawlessly. If not, it might result in subpar predicted outcomes or even a model that doesn't provide any relevant information at all. To address some of the aforementioned RNN model's drawbacks, researchers have created more advanced varieties of RNNs, including the following:

i. The Long Short-Term Memory (LSTM).

ii. The Bidirectional Long Short-Term Memory (BLSTM).

iii. The Gated Recurrent Unit (GRU).

iv. The Bidirectional Gated Recurrent Unit (BGRU).

The most advanced method for learning sequences is known as Long Short-Term Memory Networks (LSTMs). Hochreiter and Schmidhuber presented the LSTM for the first time, and subsequent publications like References [96] and [97] improved upon and popularized it. The LSTMs are a unique type of RNN that have been developed to solve the long-term dependence issue in addition to the regular RNN's vanishing and ballooning gradient issues. This was accomplished via a method known as cell states, which is according to a gating system to offer a framework with memory. The latter is employed to regulate reading, writing, and erasing (forgetting) the written data from the memory state [98].

The cell state and the gating system are the foundation of the main principle of LSTM. In theory, during sequence processing, pertinent data will be stored in the cell state. Hence, even information from earlier temporal steps will enable subsequent actions to be taken, reducing the influence of short-term memory. The gating mechanism regulates whether data is added to or removed from the cell state. Three different sorts of gates are included in this system, which will teach users what knowledge is crucial to remember or forget throughout training. The forget gate, input gate, and output gate are these gates [99].

The LSTM structure is illustrated in *Figure 10* with $\boldsymbol{h}^t \in R^M$ and $\boldsymbol{c}^t \in R^M$ hidden state vector (also known as the output vector of the LSTM unit) and the cell state vector at time t, respectively. M stands for the number of nodes (hidden units).
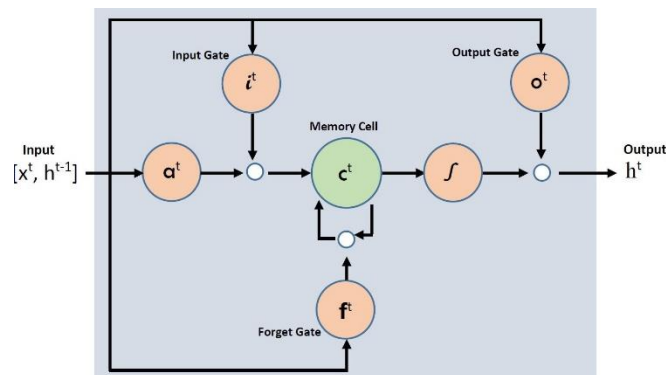

Figure 10 Schematic of LSTM [99].

The sensor data x^t as well as $\boldsymbol{h}^{t-1}$ and $\boldsymbol{c}^{t-1}$ from time (t-1) will be the input to the LSTM. The gating system, an inner mechanism is according to the following gates, regulates the information flow within the inner cell unit:

i.   Forget gate: A forget gate, indicated by $\boldsymbol{f}^t \in R^M$, that determines whether

certain items should be kept or forgotten [100]. The input to this gate consists of the current input and the previous hidden state, which are then multiplied by the weight matrices and a bias is added. The output is then passed through the sigmoid function, which creates a vector with values ranging from 0 to 1, one for each number in the cell state. In essence, the sigmoid function is in charge of selecting which data to keep and which to discard. The closest to 0 therefore indicates forgetting, whereas the closest to 1 indicates holding.

     ii.   Input gate: A cell state update process based on $\boldsymbol{h}^{t\text{-}1}$ and x^t is managed by an input gate $\boldsymbol{i}^t \in R^M$ [100]. According to the forget gate, the *sigmoid* function decides the important (1) and the unimportant after it receives the current input and the prior concealed state (0). Also, a vector containing every conceivable value that may be added to the cell state is created by passing the current input and the previously concealed state through the *tanh* function (output values range from -1 to +1). Next, the *sigmoid* will choose which data to retain from the output of the tanh by multiplying both the *sigmoid* and *tanh* outputs, and these beneficial updates will then be added to the cell state.

     iii.   Output gate: An output gate that evaluates the subsequent value of the hidden state is designated by the symbol $\boldsymbol{o}^t \in R^M$ [100]. The cell state is used with the tanh function to create a vector with values between -1 and +1, and the current input and the previous hidden state are then supplied to the *sigmoid* function to control the vector's output values (from the *tanh*). The output and hidden state for the following cell is obtained by multiplying the previous output by the vector (which was the result of *tanh*).

     The LSTM cells are implemented according to the following equations [101] at every step *t*:

$$i^t = \sigma(W_i x^t + U_i \boldsymbol{h}^{t-1} + \boldsymbol{b}_i), \qquad (22)$$

$$o^t = \sigma(W_0 x^t + U_0 \boldsymbol{h}^{t-1} + \boldsymbol{b}_0), \qquad (23)$$

$$\boldsymbol{f}^t = \sigma(W_f x^t + U_f \boldsymbol{h}^{t-1} + \boldsymbol{b}_f), \qquad (24)$$

$$\boldsymbol{a}^t = tanh(W_c x^t + U_c \boldsymbol{h}^{t-1} + \boldsymbol{b}_c), \qquad (25)$$

$$\boldsymbol{c}^t = \boldsymbol{f}^t \circ \boldsymbol{c}^{t-1} + \boldsymbol{i}^t \circ \boldsymbol{a}^t, \qquad (26)$$

$$\boldsymbol{h}^t = \boldsymbol{o}^t \circ \tanh(\boldsymbol{c}^t), \qquad (27)$$

When the weight matrices are made up of the words W_i, W_0, W_f, and $W_c \in R^{M \times L}$ as well as terms U_i, U_0, U_f, and $U_c \in R^{M \times M}$; Biases are represented by the terms $\boldsymbol{b}_i$, $\boldsymbol{b}_0$, $\boldsymbol{b}_f$, and $\boldsymbol{b}_c \in R^M$; the number of input features is represented by L; The term "*tanh()*" stands for the activation function, while the operators "*o*" and "*σ*" stand for an entry-wise product action and element-wise multiplication of two vectors, respectively. The LSTMs have been effectively used in a variety of applications, including image captioning [102], handwriting recognition [103], hand action recognition [104], speech recognition [105], natural language processing [106], and human action recognition.

Because the LSTM was so effective in PHM applications and related disciplines, several other strategies have been put forth. To detect hidden patterns and learn complex features within the sensor and operational data with multiple operating conditions, fault, and degradation models, Zheng et al. [107] presented an LSTM-based model for RUL prediction. This model uses multiple layers of LSTM cells along with standard feed-forward layers. Vanilla LSTM neural networks, a powerful method in the field of natural language processing, were utilized by Wu et al. [108] to construct a model for RUL prediction. A dynamic difference

approach is suggested in addition to standard LSTM neural networks to extract additional features from unprocessed medical monitoring data. The Long Short-Term Memory based Encoder-Decoder (LSTM-ED) approach was presented by Malhotra et al. [109] for calculating the unsupervised health index (HI) of a system according to the multi-sensor time-series data (from which the RUL may be computed). The multivariate time-series pertaining to a system's healthy state is first reconstructed using the LSTM-ED, which is then trained to do so. The reconstruction error is then utilized to calculate the HI, which is subsequently utilized to RUL prediction. By utilizing the Long Short-Term Memory (LSTM) approach to successfully learn features from multivariate time-series data and then capture long-term dependencies via the recurrent actions and gate mechanism, Lei et al. [101] demonstrated a failure diagnostic for wind turbines. A method for supercapacitor life estimation was put up by Zhou et al. [110] by leveraging the LSTM to capture long-term dependencies of a deteriorated supercapacitor. The LSTM was employed by Liu et al. [111] to provide a technique for proton exchange membrane fuel cell RUL estimation. For the reconstruction and smoothing of the data, this approach additionally employs periodic interval sampling and locally weighted scatterplot smoothing. In order to create a feature set based on time element, Wang et al. [112] retrieved feature variables from the time domain, frequency domain, and time-frequency domain. They then chose the values that best described the bearings degradation behavior. This feature set was used by the LSTM during training and prediction of the rolling bearing's RUL. A deep long short-term memory was suggested by Wu et al. [113] as a means of forecasting the RUL of turbofan engines. The suggested method mixes time series data from several sensors and finds the long-term

relationships between sensor readings that are concealed for RUL estimation. The grid search methodology has also been used to identify the ideal model variables.

2.5 PEMFC prognostics literature review

The PEMFC stack is an energy converter with an excessive amount of internal complexity. Isolating the relevant factors would be fairly challenging due to the interaction and effect of many operational circumstances and parameters. Another way of saying that, it can be challenging to perform precise prognostics due to the great complexity of the fuel cell stack. The following are the key prognostications in PEMFC today:

1)   Data collecting level (tough to continuously monitor some interesting variables);

2)   Degree of prognosis (there is no common standard for PEMFC prognostics);

3)   Validating degree (the aging mechanisms on auxiliaries maybe ignored).

There haven't been many studies in recent years discussing the prognostic techniques utilized on the issue of PEMFC prognostics:

A PEMFC prognosis based on a particle filter architecture was put out in [114]. The RUL estimation of two fuel cell stacks was achieved using the particle filter, which was the primary contribution of this study. Three state models were set up in the model (linear model, logarithm model, and exponential model). These three models were evaluated and contrasted. According to the findings, the logarithm model would provide the most accurate prognostic information (RUL estimation error of 90h in a 1000h case). To the researchers' knowledge, the particle filter occasionally experiences particle depletion during operation,

and typically, to provide accurate prediction results, the particle filter requires a large amount of data.

To obtain the PEMFC prognostics, Morando et al. [115] presented an Echo State Network (ESN) technique. The researcher utilized the stack output voltage data to forecast how the PEMFC stack's output performance would deteriorate. The ESN is a method for quick learning, and it used direct and parallel structures to complete its prognostics. Nevertheless, setting up a few training variables for the prediction algorithm would be necessary. Moreover, altering preset settings may result in inconsistent predictions.

A data-driven methodology was put out by Silva et al. [116] to forecast the voltage fluctuation of two PEMFC stacks. The online prognosis in this study might be the prediction made by the Adaptive Neural Fuzzy Inference System (ANFIS). The natural aging portion of the training data for aging voltage and the external perturbations were separated by the author into two components for this work. The ANFIS forecast, though, is dependent on laborious iterative learning processes. The size of the data would affect the computing time. In addition, the ANFIS uses a soft computing strategy. The volume of experimental data and the number of initialization variables have a direct impact on the difficulty of the training method.

To determine a PEMFC stack's EIS (Electrochemical Impedance Spectroscopy) impedance, Vianna et al. [117] suggested a regression-based method. The prediction issue was approached using the linear regression method and a higher-order polynomial regression. Using the fitted impedance values, the training ranged from 0 to 515 hours. The

experimental results on impedance measurements made at four distinct frequencies and times-5.18 Hz, 505 Hz, 50 MHz, and 789 MHz-were used to confirm the results. These measurements were made at 685 hours, 823 hours, and 991 hours. In this impedance prediction scenario, the findings indicated greater prediction performance using linear regression. This could be because the impedance shifting profile over time has very few non-linear deterioration components.

Specifically, Hochstein et al. [118].'s illustrations of the Regime Switching Vector Autoregressive (RSVAR). The shifting dependence structures of multivariate time series may often be modeled using this approach. The prognostic scenario of a constant output PEMFC stack, with datasets comprising a range of characteristics like the stack voltage, current, inlet/outlet temperature for the fuels, etc., was briefly discussed by the researcher at the conclusion of the article. The projected outcome seemed good. Nevertheless, for training and prediction, this system would require several operational variables and quantifiable data. A big dataset is typically required if one wants accurate prediction results.

A PEMFC prognosis of a PEMFC stack employing a particle filter architecture was described by Kimotho et al. [119]. In this article, the "self-healing component" was included in the prediction scenario. The PEMFC stack's output performance would automatically recover following measurement of the data every predetermined period of time during aging thanks to self-healing. With the self-healing element applied during prediction, the results of the estimation were acceptable.

A method called the Equivalent Circuit Model (ECM) was put out by Kim et al. [120] to forecast how two PEMFC stacks' impedance would change over time. Generally, the model would comprise 10 variables for a typical ECM representation of a PEMFC stack in [120]. To reduce complexity, the author reduced the model to a 4-parameter model. As some of those values were not intended to be fixed or constant for this simplified model, it is somewhat debatable whether or not it is acceptable. In actuality, to our understanding, the double-layer capacity will gradually decline over time and is closely tied to the ECSA. This variable, nevertheless, was programmed to be fixed and eliminated from the prognostic model.

Two model-based methods for the estimation of PEMFC stack performance degradation were shown by Lechartier et al. [121]. The degradation propensity of the polarization curve was predicted using a static model based on the Butler-Volmer equation. Moreover, a dynamic model was developed using an equivalent circuit model to anticipate the EIS impedance deterioration tendency during long-term operation. Nonlinear regression was used to adjust both models to account for the PEMFC stack's aging. The prognostic results were encouraging, but as the models were only calibrated using data from the tested PEMFC stack, their applicability to other stacks is uncertain.

Bressel et al. [122] suggested an Extended Kalman Filter-based observer-based prognostic model for PEMFC (EKF). The time-varying characteristic and derivative, that might depict the aging of the cell, were estimated using the observer. The approach that was developed produced accurate predictions of voltage deterioration under various load circumstances. The efficiency of the RUL prediction was also demonstrated. It's also

intriguing that the author claimed that throughout extended operation (more than 1000 hours), the exchange current density would not vary.

Table 2 PEMFC prognostics literature review.

Prognostics class	Approach	Monitored variable	Year	Reference
Data driven	Particle filter	Stack voltage	2013	[114]
Data driven	Echo State Network	Cell voltage	2014	[115]
Data driven	Adaptive Neuro Fuzz Inference	Stack voltage	2014	[116]
Data driven	Regression	EIS Impedance	2014	[117]
Data driven	Switching Vector Autoregressive	Stack voltage	2014	[118]
Data driven	Particle Filter	Stack voltage	2014	[119]
Hybrid	Equivalent Circuit Model	EIS Impedance	2015	[120]
Model based	Equivalent Circuit Model	Polarization curve / EIS Impedance	2015	[121]
Data driven	Extended Kalman filter	Stack voltage	2016	[122]

Table 2 lists each study project's features. We could see from this table that the data-driven approach is more common than the other two. This is due to the fact that, when it comes to PEMFC prognostics, data-driven methodologies are often more useful than others. Furthermore, the stack voltage was mostly in use. This is because, especially in a continuous operating profile, the stack voltage is the parameter that is easiest to measure in order to evaluate output performance or condition of health.

Nevertheless, each of the works may have one or more of the following drawbacks, which apply to the majority of data-driven techniques in the literature:

1. High computational requirement;

2. Large dataset required for training;

3. Insufficient validation under varying load situations;

4. Generalizations about various stacks and circumstances.

2.6 Thesis overview

This thesis aims at developing data-driven methodologies like as artificial neural networks (ANNs) and deep learning techniques to predict fuel cell degradation. We employ the ANN, deep neural networks (DNN), and long short-term memory (LSTM) models, to forecast PEMFC stacks' voltage deterioration and calculate their RUL.

2.6.1 Objectives

The following are the precise goals:

1) Collect real-world experimental data on the voltage degradation of PEMFC stacks under various operating conditions.

2) Develop and evaluate ANN models with different architectures and hyperparameters to predict the voltage degradation of PEMFC stacks.

3) Develop and evaluate DNN models with different architectures and hyperparameters to predict the voltage degradation of PEMFC stacks.

4) Develop and evaluate LSTM models with different architectures and hyperparameters to predict the voltage degradation of PEMFC stacks.

5) Compare the performance of different models and identify the most effective model for prognostics of PEMFC stacks.

2.6.2 Methodology

The proposed methodology for this research involves the following steps:

1) Data collection: Collect real-world experimental data on the voltage degradation of PEMFC stacks under different operating conditions.

2) Data preprocessing: Clean and preprocess the data by removing outliers, filling missing values, and normalizing the data.

3) Model development: Develop ANN, DNN, and LSTM models with different architectures.

4) Model evaluation: Evaluate the performance of different models using metrics such as mean squared error (MSE), root mean squared error (RMSE), and R-squared (R2) on test data.

5) Model comparison: Compare the performance of different models and identify the most effective model for prognostics of PEMFC stacks.

2.6.3 Expected outcomes

The expected outcomes of this research are as follows:

1) Development of data-driven models, including ANN, DNN, and LSTM, for

predicting the voltage degradation of PEMFC stacks and estimating their RUL.

2) Comparison of the performance of different models and identification of the most effective model for prognostics of PEMFC stacks.

3) Validation of the proposed models using real-world experimental data and demonstration of their effectiveness in practical applications.

4) Contribution to the field of PEMFC prognostics and promotion of the use of data-driven methods for more accurate and reliable prognostics.

Chapter 3: Artificial Neural Network

An effective and popular technique for function approximation and pattern recognition is the Artificial Neural Network (ANN). ANNs are able to learn from and adapt to complicated and nonlinear connections in data since they are based on the structure and operation of the human brain. Several industries, including banking, engineering, healthcare, and many more, have effectively used the ANN approach.

This chapter's goal is to show how the ANN approach may be applied to a straightforward function before applying it to the prediction of PEMFC degradation. At the beginning, we'll provide a straightforward function and demonstrate how to train an ANN model to forecast its results. The use of the ANN approach to anticipate PEMFC degradation, which is a key difficulty in the field of fuel cells, will be covered next. An effective and popular technique for function approximation and pattern recognition is the artificial neural network (ANN). ANNs are able to learn from and adapt to complicated and nonlinear

connections in data since they are based on the structure and operation of the human brain.

3.1 Approximation of a Sinusoidal Function

The function we want to predict is $f(x_1, x_2) = \sin(1 + x_1 x_2)$, where x_1 and x_2 are input variables. We have 1000 samples for x_1 and 1000 samples for x_2. The first input variable x_1 is a linearly spaced vector from 0 to 2π with 1000 points and the second input variable x_2 is generated by adding 1000 random samples between 0 and 2π to a vector that contains two fixed values (0 and 2π). The output variable $f(x_1, x_2)$ is calculated by applying the sinusoidal function to the input variables.

The ANN is trained using the Levenberg-Marquardt backpropagation algorithm with a trainlm training function, and a two-layer architecture consisting of 32 and 16 neurons in the first and second hidden layers, respectively as shown in Figure 11. The chosen performance function is the mean squared error (MSE), and the training is performed for 10000 epochs. Next, we split the data into training, validation, and test sets. We use 70% of the data for training, 15% for validation, and 15% for testing.
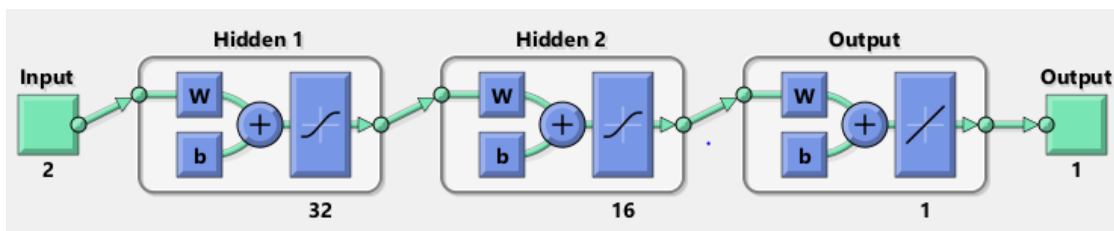
Figure 11 Sinusoidal function approximation architecture of ANN.

The plot of the prediction of the $\sin(1 + x_1 x_2)$ function using ANN is shown in *Figure 12*. The blue line represents the actual values of the $\sin(1 + x_1 x_2)$ function, and the orange point represents the predicted values obtained from the ANN model. The graphic clearly

shows that the projected values nearly match the actual values, demonstrating how well the ANN captured the underlying patterns in the data.
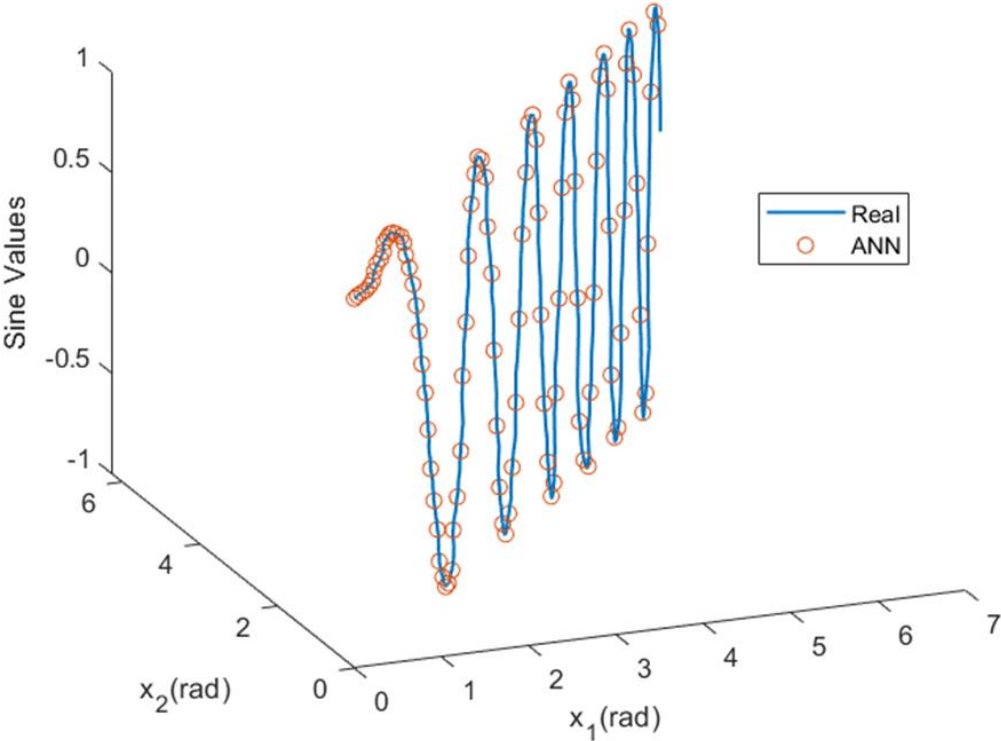

Figure 12 ANN prediction plot for $in(1 + x_1 x_2)$.

We decided to employ a feedforward neural network to solve this problem, which implies that the inputs are sent through the network in a forward manner without any feedback loops. The network's design consists of two hidden layers, each of which has a certain number of neurons, followed by an output layer. By testing, the number of neurons in the hidden layers is established and is dependent on the difficulty of the issue.

Regression plots can be used in addition to the prediction plot to assess how well the ANN model is working. In a regression plot, the predicted values and the actual values of the output variable are compared and plotted on a scatter plot. All the points in an ideal model would be on a straight line with a slope of 1.

Figure 13 depicts the regression curve for the $\sin(1 + x_1 x_2)$ function using the ANN model. The scatter plot displays the actual values on the x-axis and the expected values of the $\sin(1 + x_1 x_2)$ function on the y-axis. The scatter plot's dots are densely grouped around the line that best fits them; this line is a straight line with a slope of 1. This shows that the ANN model can correctly anticipate the output values and has identified the underlying patterns in the data.
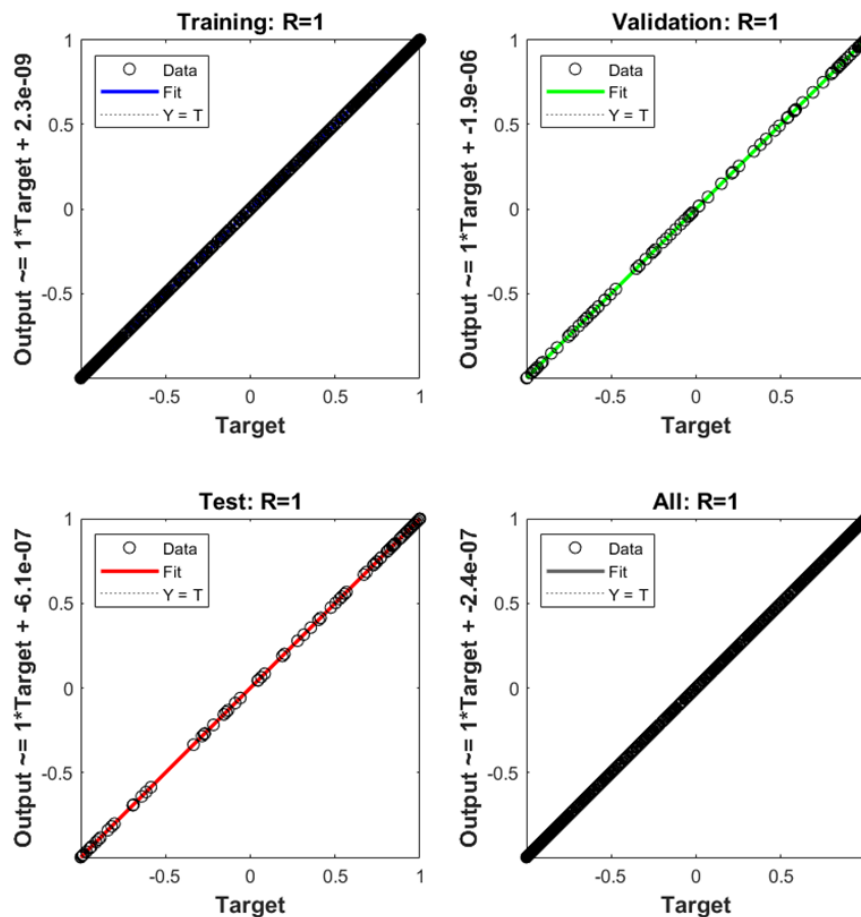

Figure 13 ANN-based regression curve for $in(1 + x_1 x_2)$.

Overall, the use of ANN on the $\sin(1 + x_1 x_2)$ function has shown how well it can identify the underlying patterns in the data and forecast the output values. This gives a solid basis for utilizing ANN to forecast PEMFC degradation.

3.2 Approximation of the PEMFC degradation

The performance prediction of proton exchange membrane fuel cells (PEMFCs) is a critical issue that affects the performance and reliability of these devices. Accurately predicting of PEMFCs over time is essential for optimizing their performance and extending their lifespan.

In this part, we use data-driven approaches based on experimental results from prior research to forecast the PEMFC load current and stack voltage. Using WebPlotDigitizer, we retrieved the load current and recorded stack voltage plot data from the [123] reference and utilized this information to train and test an artificial neural network to forecast the voltage and current of PEMFC over time.

3.2.1 Case Study

The case study we are considering in this section is a research paper published in IEEE Transactions on Industrial Electronics [123]. The research paper presents an experimental study on the performance degradation of a proton exchange membrane fuel cell (PEMFC) and proposes a method for analyzing the degradation based on the load current and stack voltage signal.

The PEMFC stack used in the experiment was a commercial 24-cell stack, which consisted of multiple individual fuel cells arranged in a series configuration. Each individual cell contained an anode, a cathode, and a proton exchange membrane. The anode was typically made of a porous carbon material, and the cathode was made of a layer of platinum

or other catalyst material supported on a porous carbon substrate. The proton exchange

membrane was typically made of a perfluorinated sulfonic acid polymer, which allowed for

the exchange of protons between the anode and cathode compartments (*Figure 14*).

Figure 14 Schematic of the first case study [123].

The operating conditions of the PEMFC were controlled using an external load

resistor and a temperature-controlled water bath. The load resistor was used to vary the

electrical load on the PEMFC, which in turn affected the load current and stack voltage. The

temperature-controlled water bath was used to control the operating temperature of the

PEMFC, which the operating conditions were shown in **Error! Reference source not

found.**.

Parameter	Value
Temperature (°C)	80
Anode and cathode stoichiometry ratios	1.5-2
Absolute pressure anode/cathode (bar)	1.5
Relative humidity anode/cathode (%)	50
Nominal current density (A.cm^{-2})	0.45
Maximum current density (A.cm^{-2})	0.77

Table 3 Operating conditions of the first case study [123].

3.2.2 ANN for the first case

The data from the experimental study, including the load current and recorded stack voltage plot data, was used in our case study to predict the degradation of the PEMFC using data-driven methods. The load current and recorded stack voltage plot data was extracted using WebPlotDigitizer which shown in   and **Error! Reference source not found.** respectively.
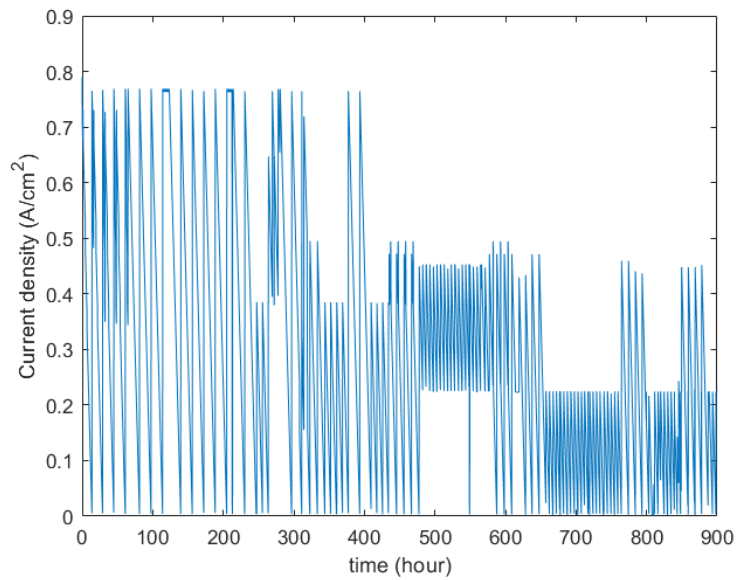

.

Figure 15 Stack voltage plot data of the first case study.

The ANN is trained using the Levenberg-Marquardt backpropagation algorithm with a trainlm training function, and a two-layer architecture consisting of 32 and 16 neurons in the first and second hidden layers, respectively (*Figure 11*). The trained ANN model's projected load current and recorded stack voltage graphs were contrasted with experimentally observed plots. The comparison charts in *Figure 17* and **Error! Reference source not found.** demonstrate that the ANN model can predict the PEMFC system's behavior with high accuracy, with good agreement between the anticipated and actual plots.
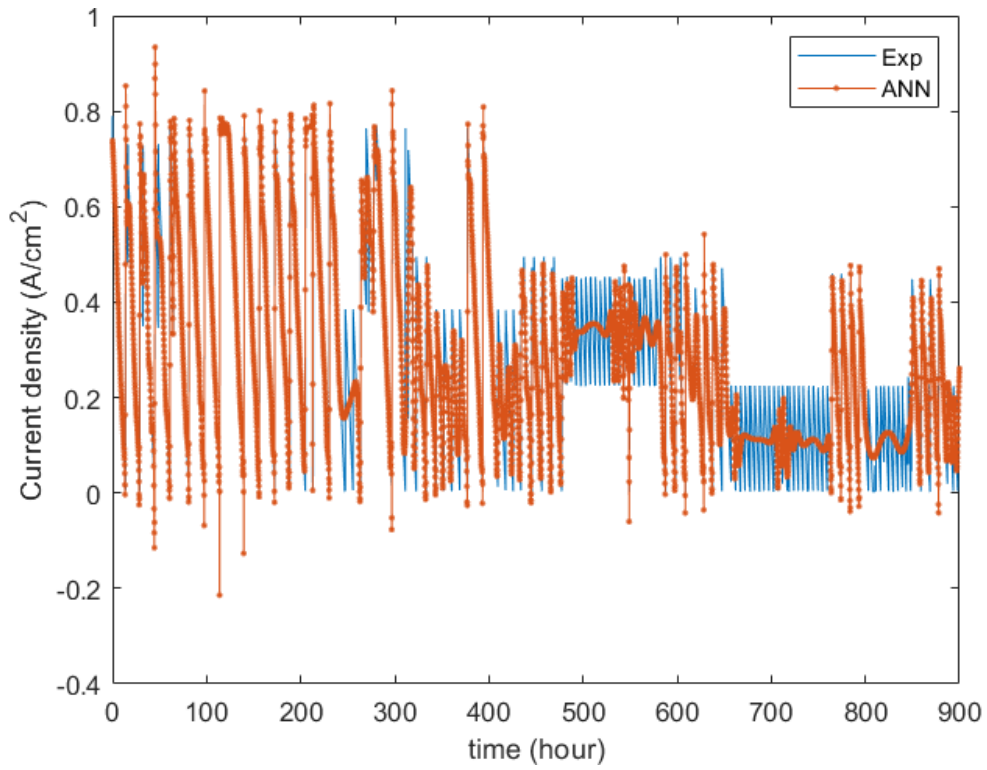
Figure 17 Comparison between experimental and ANN value (Load current).
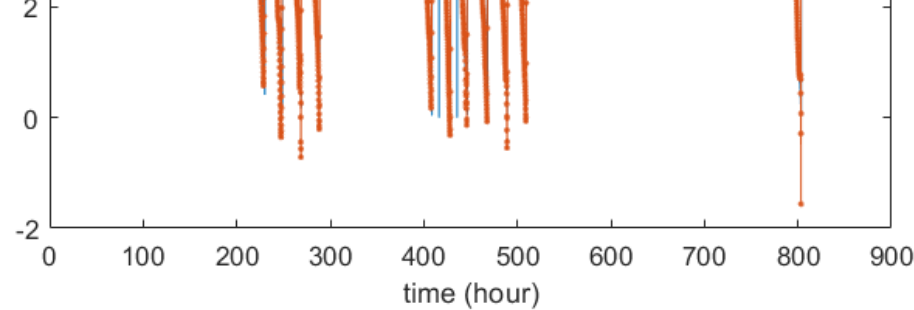
Figure 18 Comparison between experimental and ANN value (Stack voltage).

We utilized the Mean Squared Error (MSE) plot to assess how well the ANN model performed. The variance of the MSE during the ANN model's training and testing stages is seen in this graphic. The performance of the model is improved by a reduced MSE. The MSE curve for the ANN model is displayed in **Error! Reference source not found.**. The model is well-trained and not overfitting, as shown by the best validation performance of 0.0052673 at epoch 533.

A regression plot is employed to assess the relationship between the expected and actual values. The model performs better the closer the data points are to the line of perfect correlation. The regression curve for the ANN model is displayed in *Figure 20*. As we can see, there is a strong correlation between the projected and observed values, proving that the ANN model is a solid choice for predicting experimental data from the load current and recorded stack voltage plot data.
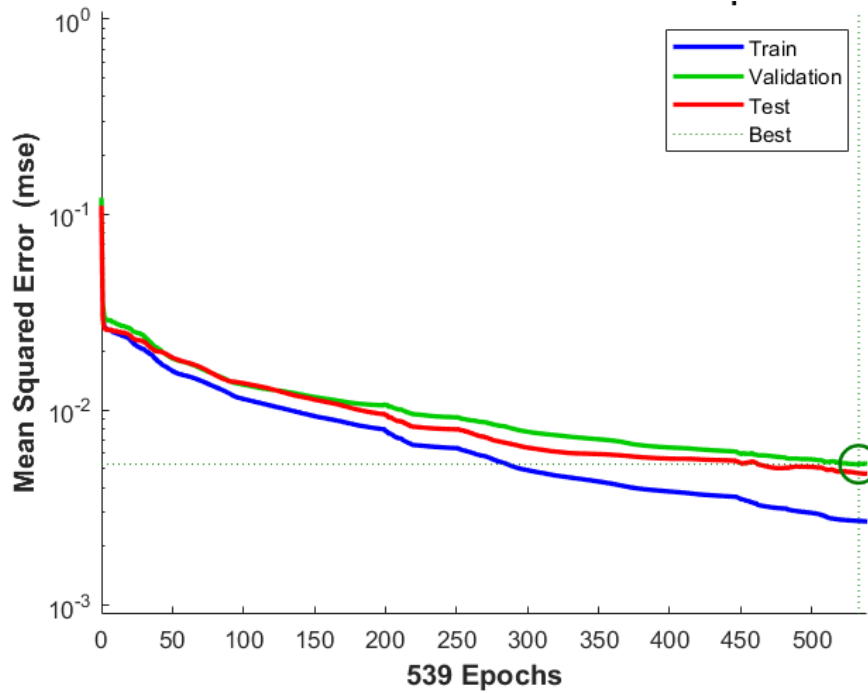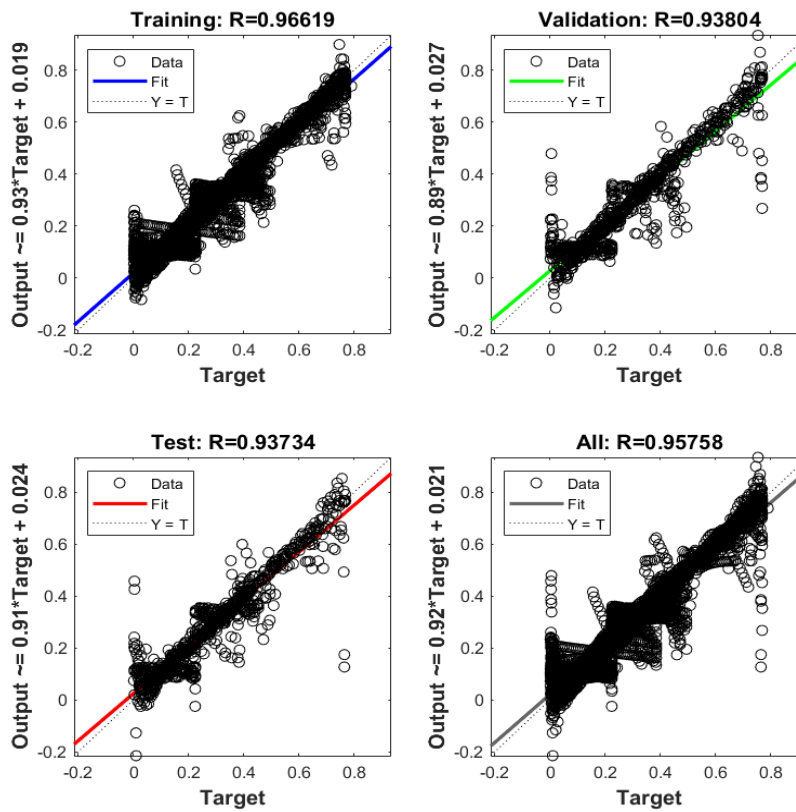
Figure 19 MSE plot of the ANN model.

Figure 20 Regression plot of the ANN model.

Chapter 4: Results and Discussion

This chapter focuses on the prediction of PEMFC degradation using data-driven methods such as ANN, DNN and LSTM. The experimental data test used in this study was obtained from the [124] reference that employed a constraint-based summation-wavelet extreme learning machine (CSW-ELM) algorithm, which is a data-driven machine learning technique that combines constraint optimization with wavelet transformation. The extracted voltage plot data from the test was used as input for the models, and the accuracy and computational efficiency of the models were compared to determine the most effective method for predicting PEMFC stack degradation.

4.1 ANN method

In the first section of the chapter on predicting the degradation of a PEMFC stack using data-driven methods, we focused on training an Artificial Neural Network (ANN) model with one hidden layer to predict the voltage degradation of the PEMFC stack. The training results of the ANN model were highly encouraging, as the model was able to accurately learn the underlying patterns in the experimental data and make accurate predictions of voltage degradation.

The MSE plot indicated that the model's error decreased with each epoch during training, indicating that the model was improving its predictions with each iteration. This showed that the model was effectively learning from the data and continuously improving its predictions and the best validation performance is 6e-5 at epoch 31 (*Figure 21*).
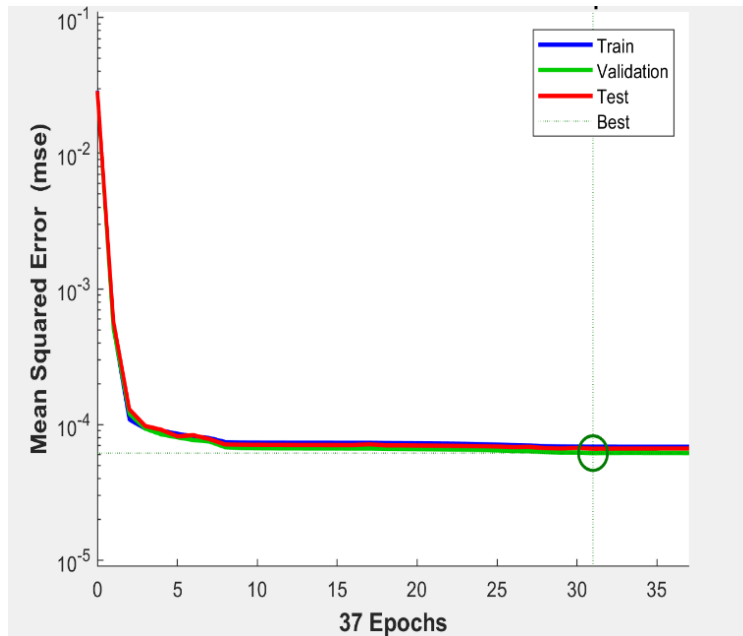
Figure 21 Mean squared error of the ANN model.

Also, the output target (fit function) in *Figure 22* showed the model's predictions compared to the actual values. The plot indicated that the model's predictions closely followed the actual values, with very little deviation. This suggested that the model was accurately capturing the underlying patterns in the data and effectively predicting the voltage degradation of the PEMFC stack.

Error! Reference source not found. showed the regression diagram and relationship between the predicted voltage degradation and the actual voltage degradation. This indicated that the model was able to capture the essential patterns in the data and accurately predict the voltage degradation.
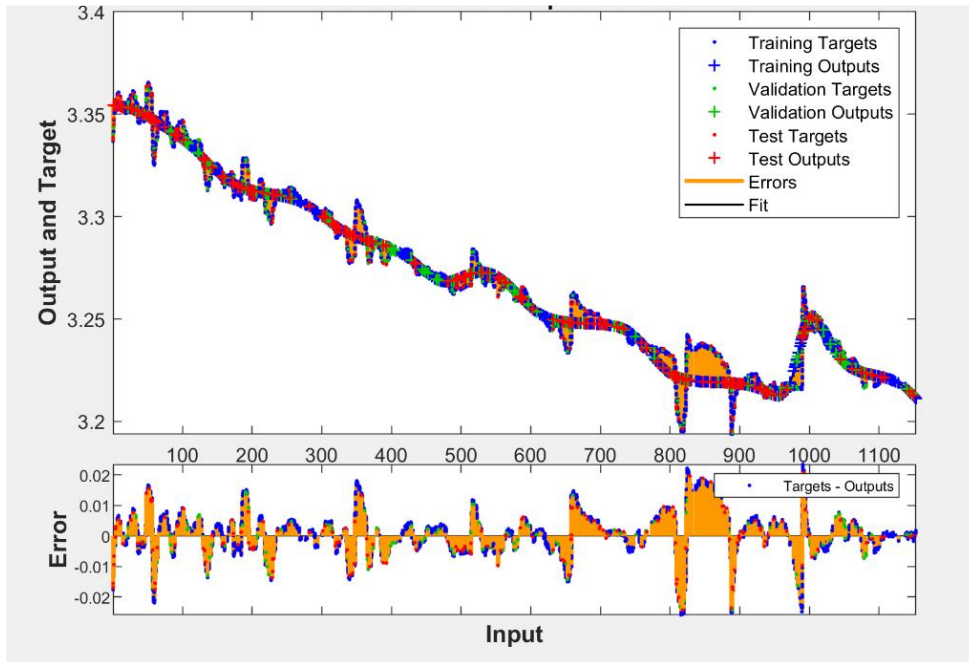
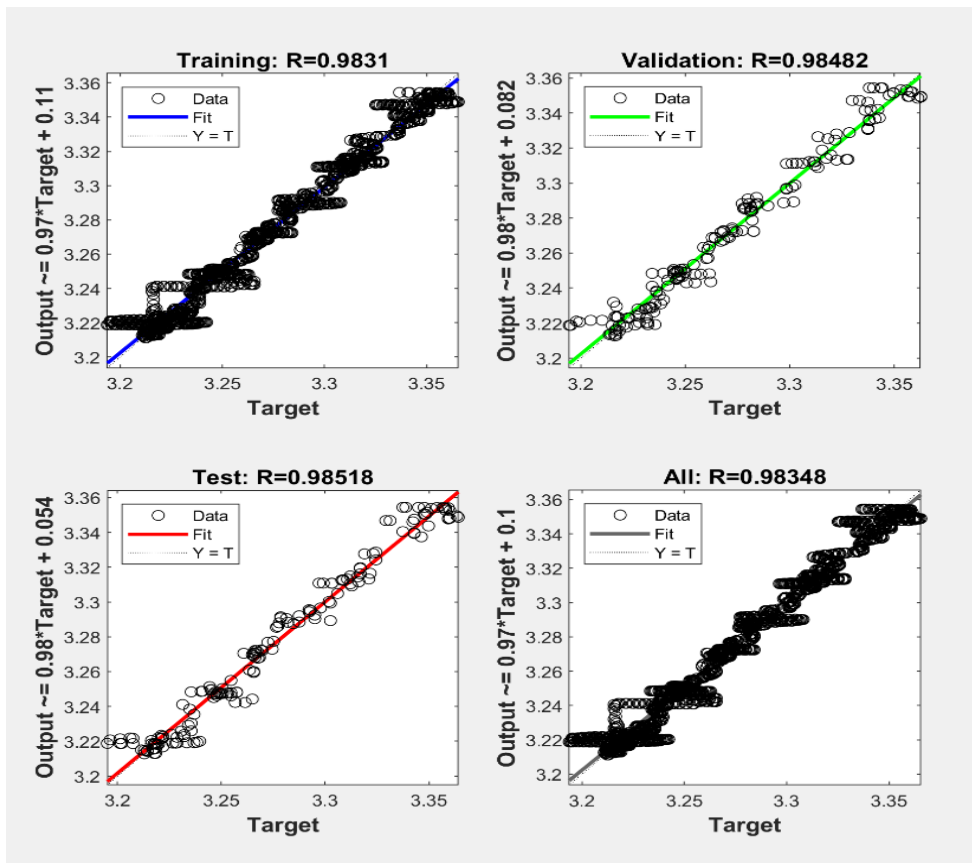*Figure 22 Fit function of the ANN model.*

Figure 23 Regression of the ANN model.

79

4.2 DNN method

Figure 23 illustrates the architecture of the DNN model, which consists of three hidden layers with 32, 16, and 8 neurons in each of the first, second, and third layers, respectively. In order to forecast the voltage degradation of the PEMFC stack, the model was trained using the same experimental data as the ANN model.
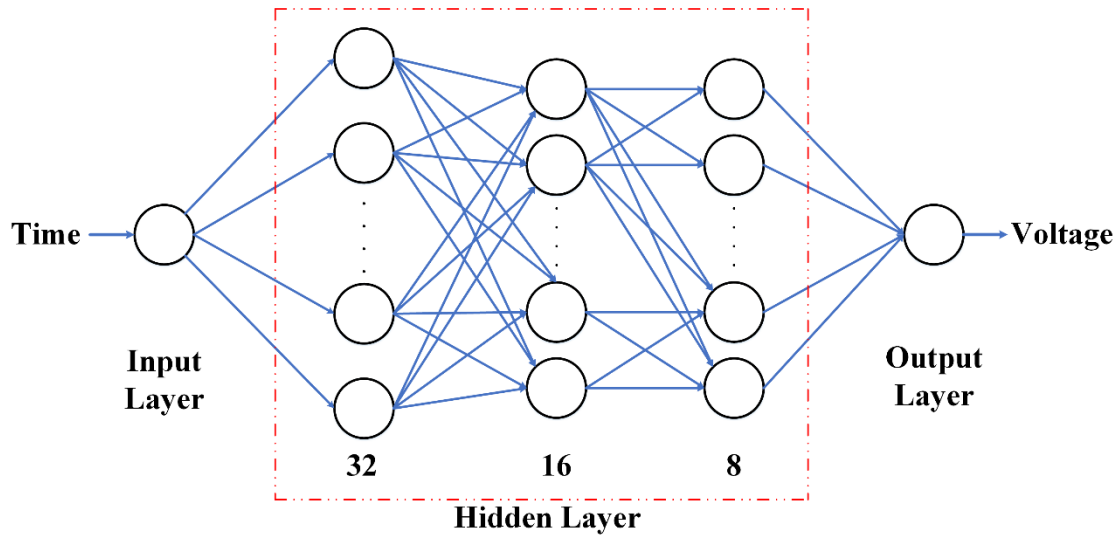

Figure 23 DNN model architecture.

The best validation performance, as shown in *Figure 24*, is 1.0494e-5 at epoch 176. At each training period, the DNN model's error dropped, according to the MSE plot, showing that the model was becoming better at making predictions. This demonstrated how the DNN model was successfully learning from the data and making predictions that were becoming better all the time.

The output target (fit function) plot in *Figure 25* demonstrated how well the DNN model's predictions matched the actual values, with very little variance. This demonstrated that the DNN model was successfully forecasting the voltage deterioration of the PEMFC

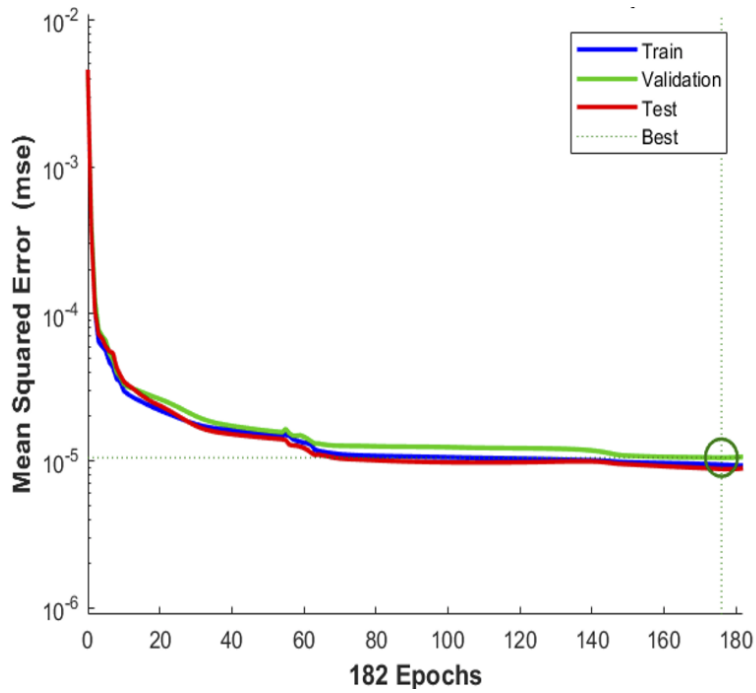stack and properly capturing the underlying trends in the data.

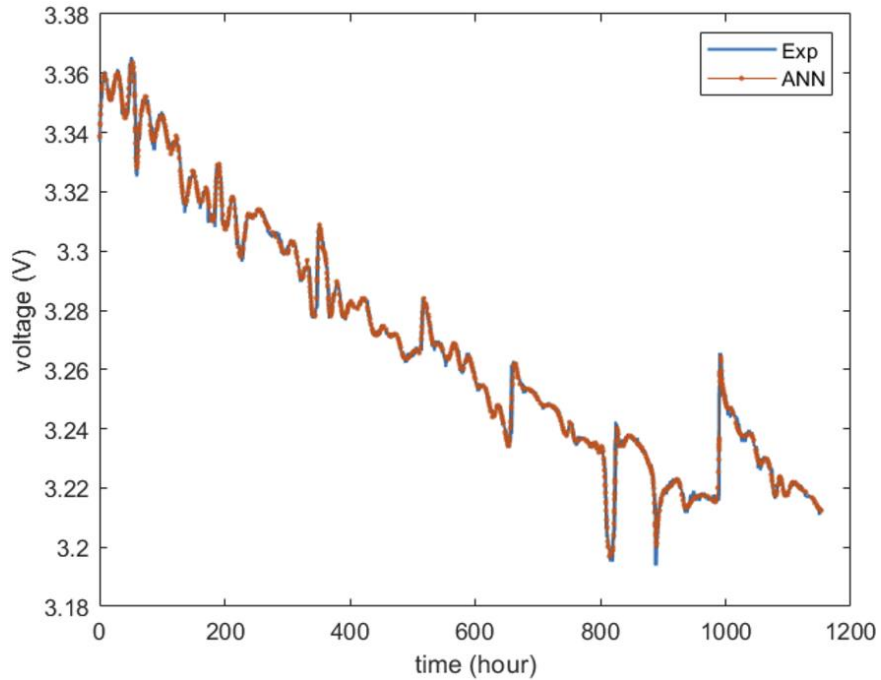*Figure 24 Mean squared error of the DNN model.*

Figure 25 Fit function of the DNN model.

81

The regression figure showed that the actual voltage degradation and anticipated voltage deterioration had a very strong linear connection. This demonstrated that the DNN model could accurately forecast the voltage decline and identify the key patterns in the data (*Figure 26*).
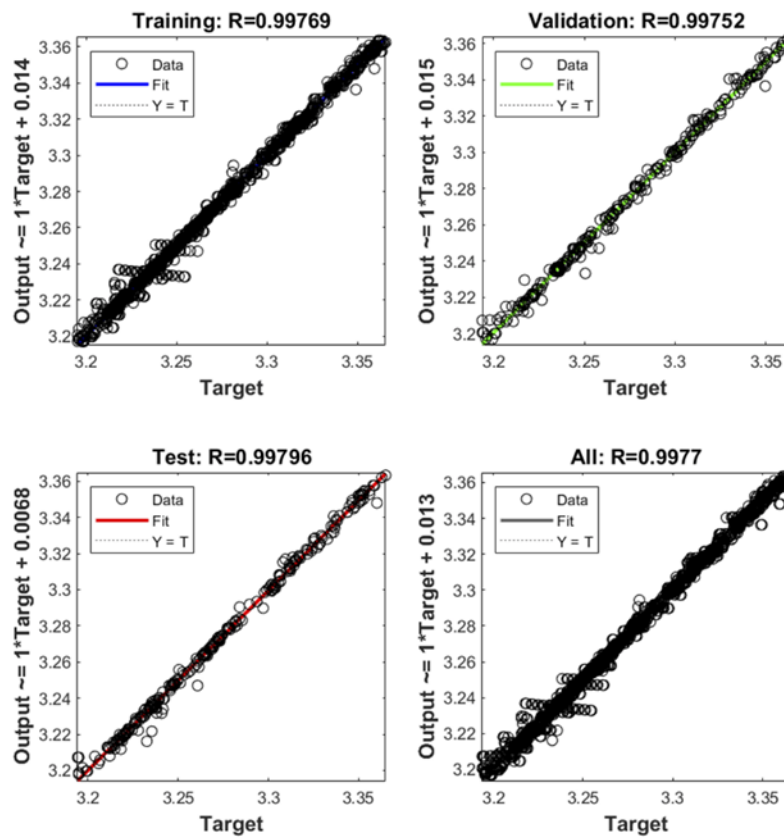

Figure 26 Regression of the DNN model.

4.3 LSTM method

The LSTM model with 4 layers and 100 epochs was further analyzed in the following portion of the chapter, and the impact of increasing the number of layers and epochs was looked at.

First, the LSTM model with 4 layers and 100 epochs was evaluated. The input to the

model was a sequence of historical data points, and the output was the predicted voltage degradation at the next time step. The prediction diagram (*Figure 27*) of this model showed a weak fit to the actual voltage degradation values, indicating that the model was not effectively capturing the underlying patterns in the data. According to the *Figure 28* ,RSME plot showed that the model's error decreased gradually with each epoch during training, indicating that the model was improving its predictions.
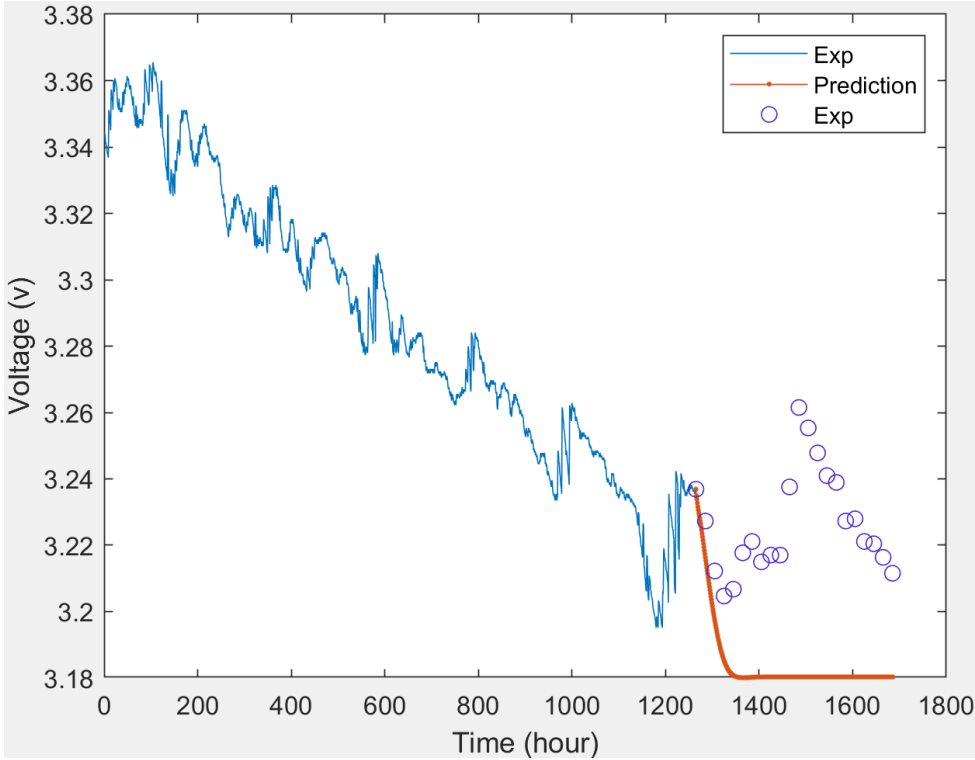

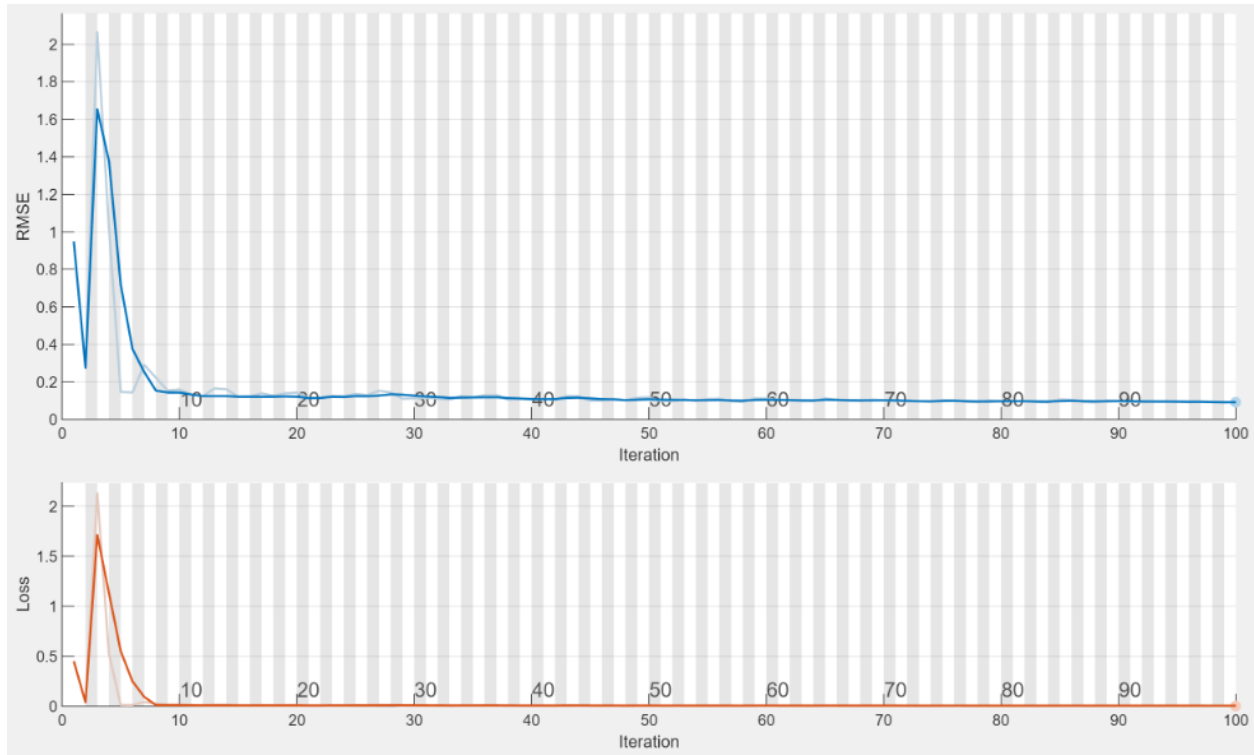*Figure 27 Fit function of the LSTM model (4 layers with 100 epochs).*

Figure 28 RMSE of the LSTM model (4 layers with 100 epochs).

Then, a 250-epoch LSTM model with 7, 6, 5, and 4 layers was trained. A series of previous data points served as the model's input, and its output was the anticipated voltage degradation at the following time step. This model's prediction curve closely matched the measured voltage degradation values, demonstrating that the model correctly identified the underlying trends in the data. The RSME error plot demonstrated that the model's error rapidly dropped with each training period, demonstrating a steady improvement in the model's predictions.

Similar to this, 250 epochs were used to train the 6, 5, and 4 layer LSTM models, and then each model's prediction curve and RSME error plots were assessed. The findings demonstrated that all models were successful in identifying the key patterns in the data, and throughout training, the error steadily decreased with each epoch.

Figure 29 Fit function of the LSTM model (4 layers with 250 epochs).

Figure 31 RMSE of the LSTM model (4 layers with 250 epochs).

Figure 31 Fit function of the LSTM model (5 layers with 250 epochs).

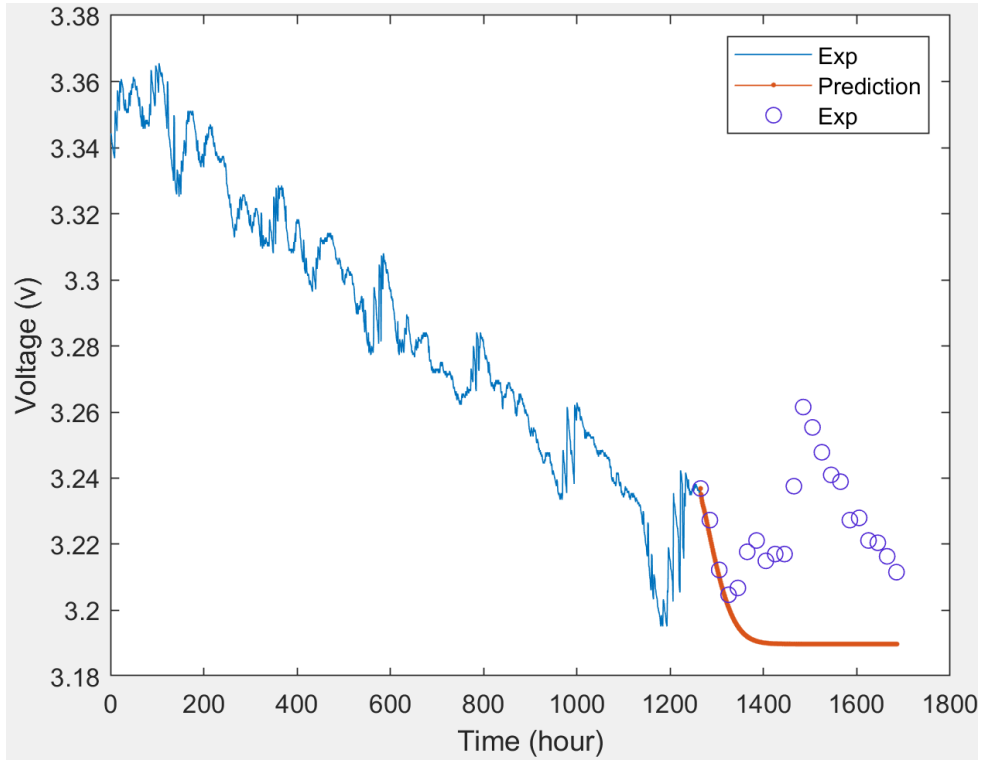*Figure 32 RMSE of the LSTM model (5 layers with 250 epochs).*

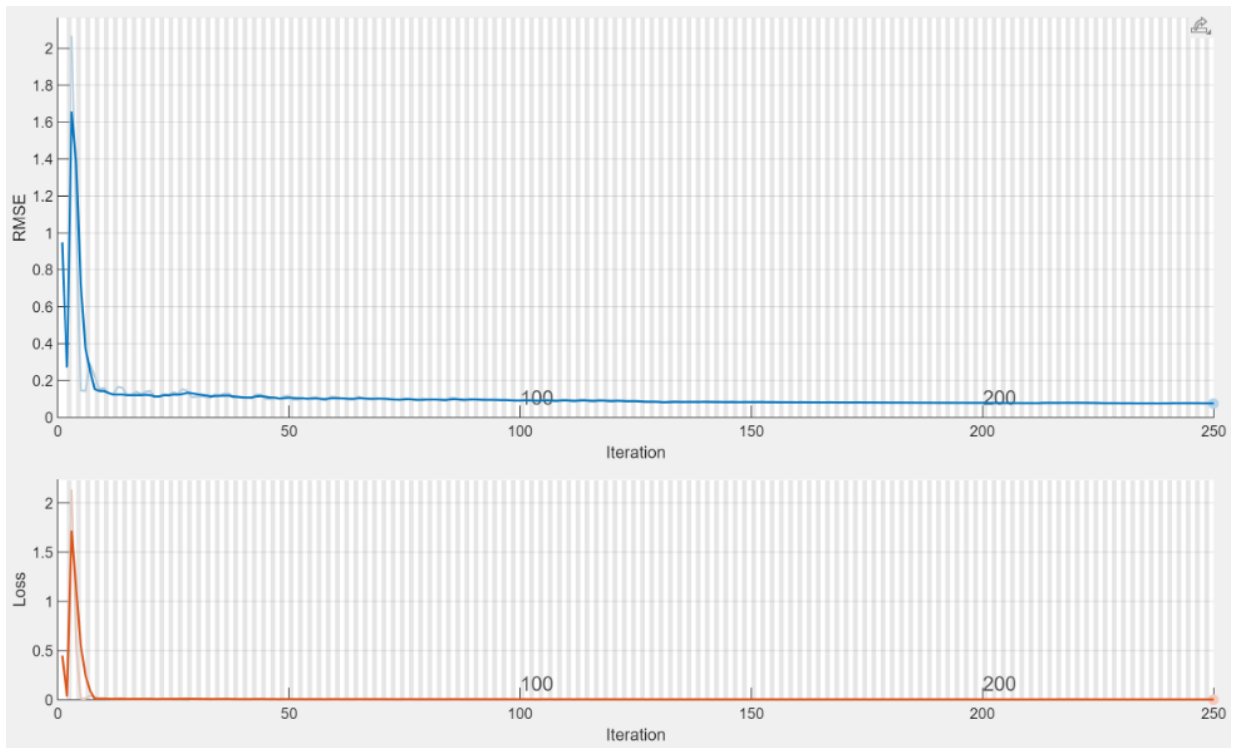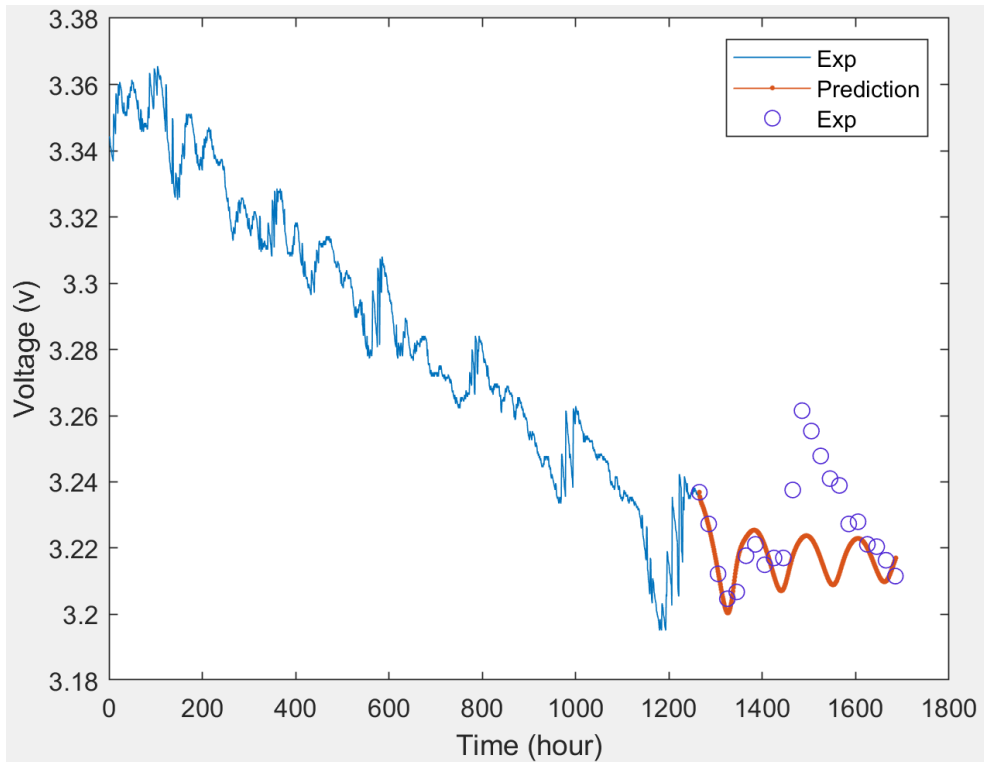*Figure 33 Fit function of the LSTM model (6 layers with 250 epochs).*
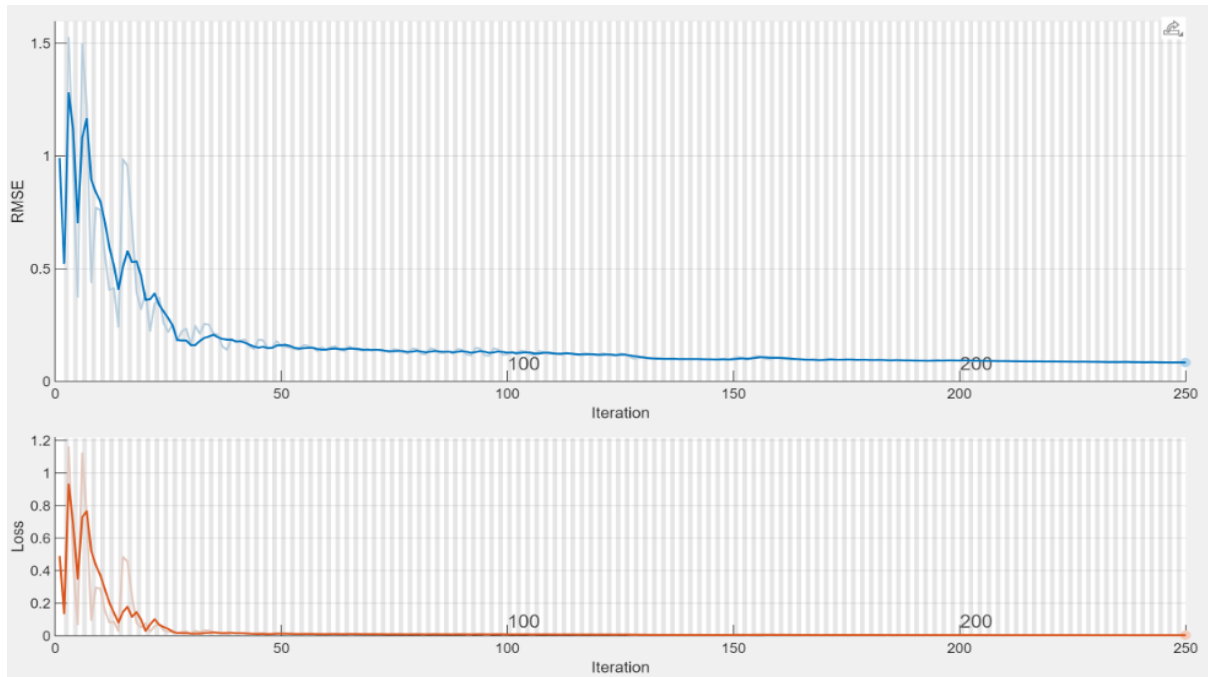
Figure 34 RMSE of the LSTM model (6 layers with 250 epochs).

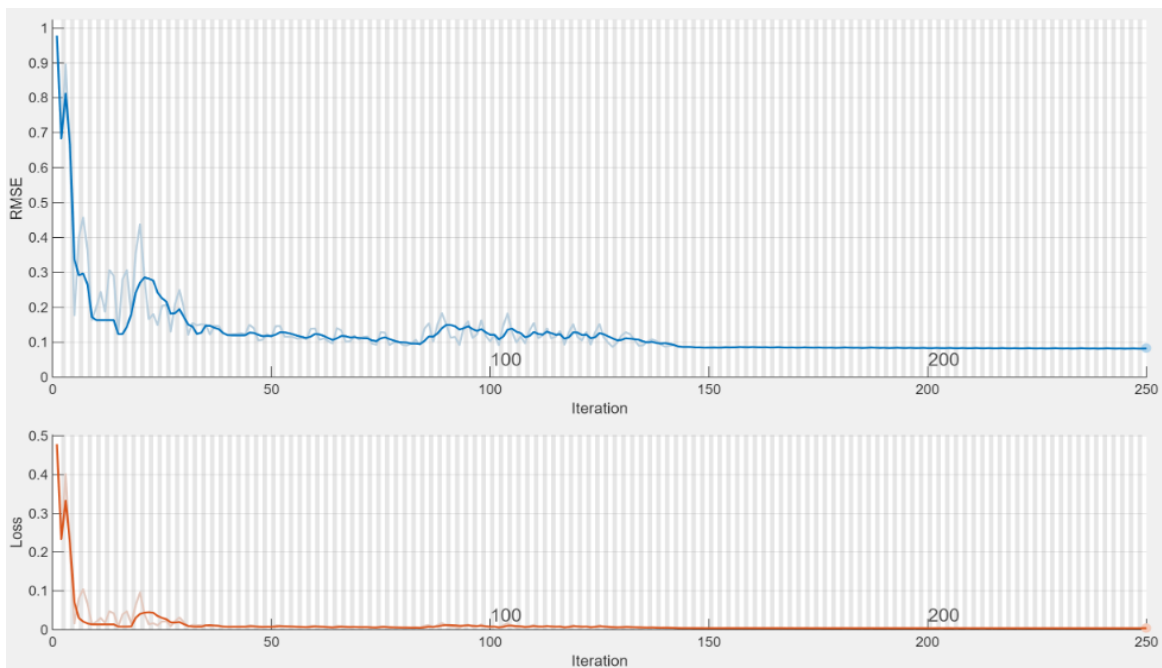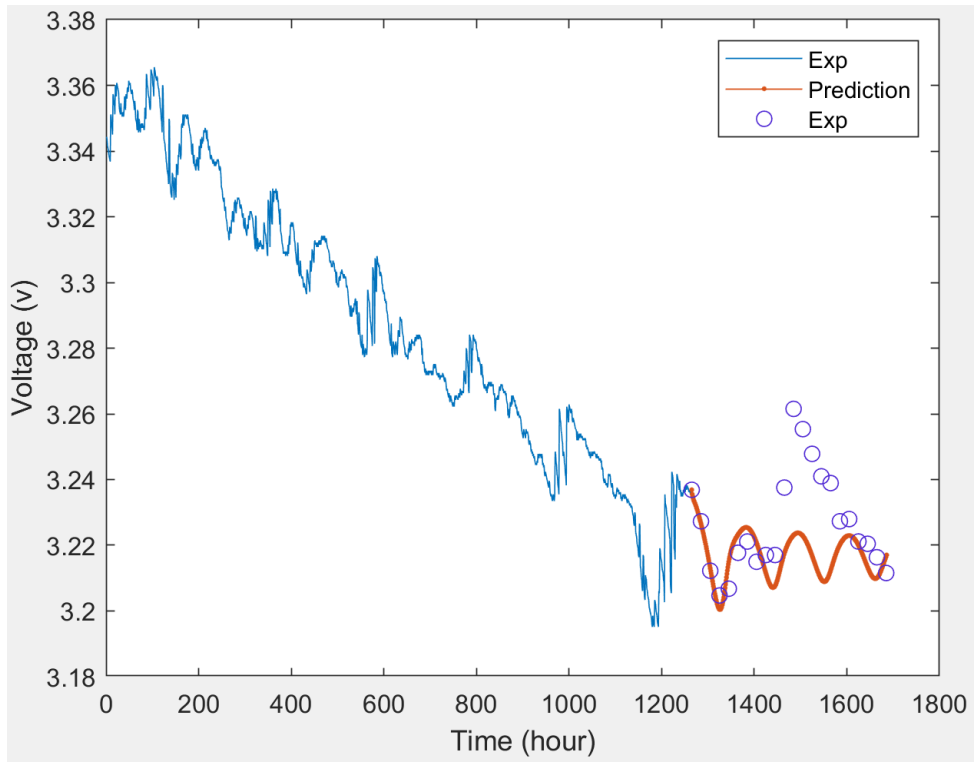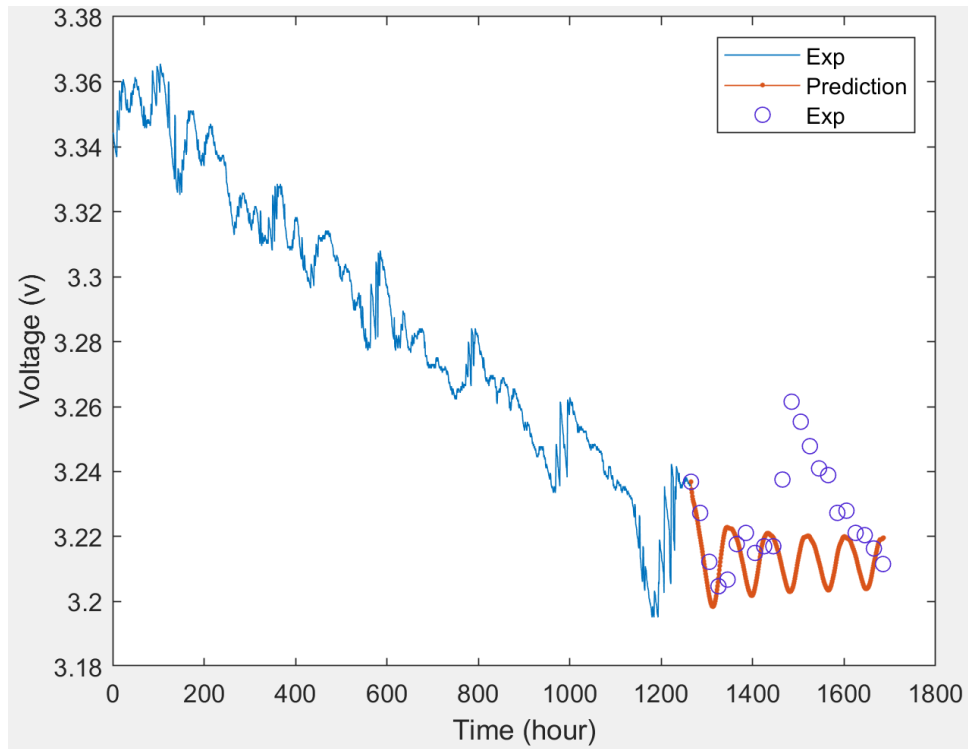*Figure 35 Fit function of the LSTM model (7 layers with 250 epochs).*
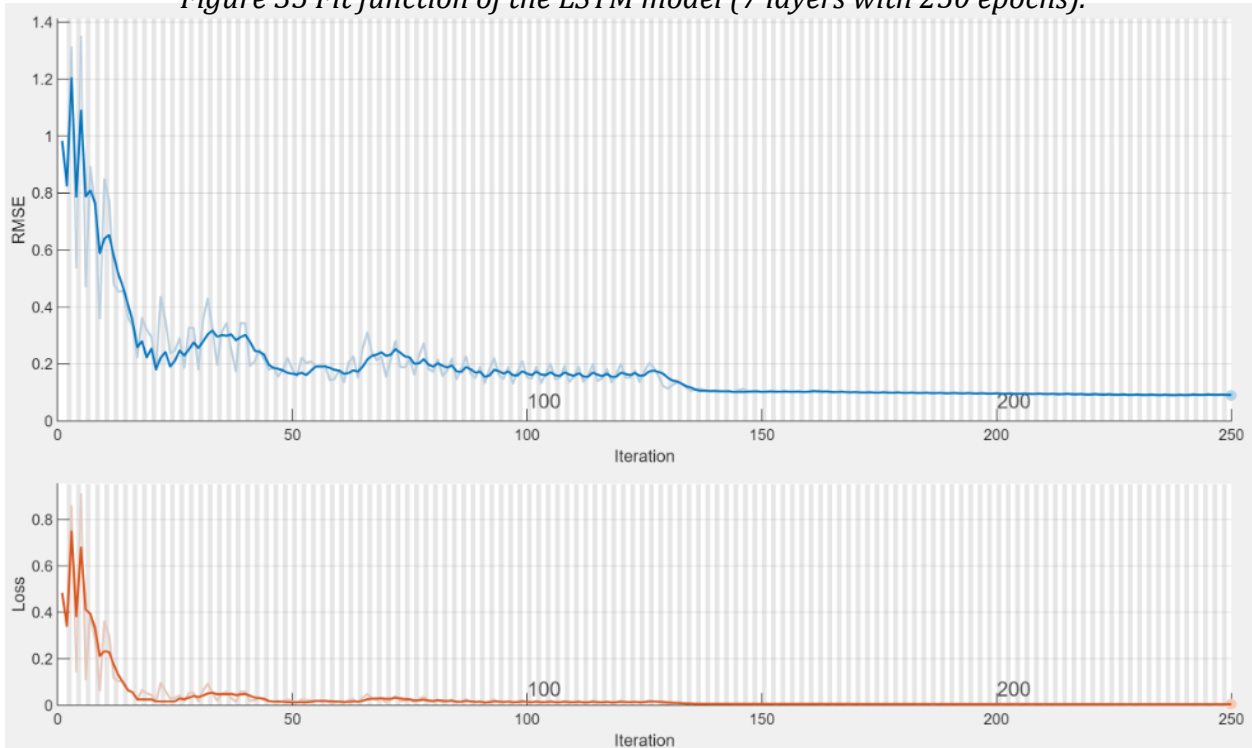
Figure 36 RMSE of the LSTM model (7 layers with 250 epochs).

The outcomes from *Figure 29* to **Error! Reference source not found.** showed that

the LSTM model's prediction ability may be enhanced by adding more layers and epochs. The danger of overfitting the model to the training data may, however, rise as the number of layers and epochs increases. To prevent overfitting, it is crucial to carefully assess the model's performance using validation data.

Also, Table 4 provides an overview of the procedures carried out and the outcomes attained by the LSTM approach for better comprehension, which demonstrates that the best case occurs in row 4.

Table 4 Overview of the LSTM models.

State	# Layers	# Epochs	# Neurons	Time	RMSE
1	4	100	200	1 min 1 sec	0.0460
2	4	250	200	2 min 27 sec	0.0189
3	5	250	400	6 min 9 sec	0.0373
4	6	250	500	8 min 4 sec	0.0169
5	7	250	700	13 min 3 sec	0.0207

Chapter 5: Conclusion

In this thesis, we investigated how to forecast the voltage degradation of proton exchange membrane fuel cell (PEMFC) stacks using data-driven techniques such as artificial neural networks (ANN), deep neural networks (DNN), and long short-term memory (LSTM) models. Using data from actual trials, we have carried out a number of tests and assessed how well these models predicted voltage decline. We have shown via trial and assessment that data-driven approaches may efficiently capture the underlying patterns in the data and offer precise voltage degradation forecasts. We have shown the promising performance of LSTM models with various numbers of layers and epochs, as well as ANN and DNN models with various numbers of hidden layers and neurons. Additionally, we have demonstrated that the model's predictive ability may be enhanced by increasing the model's complexity, such as the number of layers and epochs. To prevent over fitting, it's crucial to assess the model's performance using validation data.

5.1 Main result

The key findings show how well data-driven techniques, in particular ANN, DNN, and LSTM models, forecast the voltage deterioration of PEMFC stacks. These models are capable of capturing the underlying patterns in the data and making precise voltage degradation forecasts. We have discovered that adding more layers and neurons to the model can make it more effective at predicting the future. To prevent overfitting, it is crucial to carefully assess the model's performance using validation data. Our research also demonstrates that ANN models occasionally outperform LSTM models and are capable of accurately capturing the temporal relationships in the data. Moreover, LSTM models' prediction ability may be

enhanced by incorporating more layers and epochs.

Overall, our findings imply that data-driven approaches might enable more proactive maintenance and repair operations while offering insightful information about the health and performance of PEMFC stacks. By foreseeing the beginning of errors and deterioration before they become serious, these techniques may also be able to save downtime and maintenance costs. Our research does, however, also draw attention to the drawbacks of data-driven methodologies, such as the requirement for substantial data sets and potential over fitting. Hence, to increase the precision and reliability of prognostic approaches, future research should concentrate on creating more sophisticated machine learning algorithms and combining data-driven methods with other prognostic strategies, such as physics-based models.

5.2 Future study

Future studies could concentrate on a number of significant factors. One such component is the creation of more sophisticated machine learning techniques, such deep reinforcement learning or generative adversarial networks that can handle big and complicated datasets. Also, the exploration of alternate data sources, such as sensor data or image analysis, is a significant field for future research. These extra data sources might offer more details on the condition of the fuel cell system and possibly increase the precision of the predictive models.

Moreover, studies can concentrate on the fusion of data-driven approaches with other prognostic tools, including physics-based models or model-based methodologies. By combining these several approaches, it may be possible to analyze the health of the fuel cell

system in a more thorough and accurate manner and to make better decisions on maintenance and repair.

In addition, future study may examine the use of data-driven techniques to fuel cell system monitoring in real-time, enabling prompt and proactive maintenance responses to suspected failures or deterioration.

To summarize, more study on data-driven prognostics for PEMFC stacks is essential to enhancing the dependability and robustness of these systems. The performance and usefulness of PEMFC stacks in diverse applications might be significantly enhanced by future developments in machine learning algorithms, alternative data sources, integration with other prognostic approaches, and real-time monitoring.

References

[1] C. Spiegel, PEM fuel cell modeling and simulation using MATLAB, Elsevier2011.

[2] F. Barbir, PEM fuel cells: theory and practice, Academic press2012.

[3] Y. Wang, B. Seo, B. Wang, N. Zamel, K. Jiao, X.C. Adroher, Fundamentals, materials, and machine learning of polymer electrolyte membrane fuel cell technology, Energy and AI, 1 (2020) 100014.

[4] C.S. Gittleman, F.D. Coms, Y.-H. Lai, Membrane durability: physical and chemical degradation, Polymer electrolyte fuel cell degradation, 15 (2011).

[5] S.J. Peighambardoust, S. Rowshanzamir, M. Amjadi, Review of the proton exchange membranes for fuel cell applications, International journal of hydrogen energy, 35 (2010) 9349-9384.

[6] W. Liu, K. Ruth, G. Rusch, Membrane durability in PEM fuel cells, Journal of New Materials for Electrochemical Systems, 4 (2001).

[7] S. Yu, X. Li, J. Li, S. Liu, W. Lu, Z. Shao, B. Yi, Study on hydrophobicity degradation of gas diffusion layer in proton exchange membrane fuel cells, Energy conversion and management, 76 (2013) 301-306.

[8] H. Tawfik, Y. Hung, D. Mahajan, Bipolar plate durability and challenges, Polymer Electrolyte Fuel Cell Degradation, DOI (2012) 249-291.

[9] J. Wu, X.Z. Yuan, J.J. Martin, H. Wang, J. Zhang, J. Shen, S. Wu, W. Merida, A review of PEM fuel cell durability: Degradation mechanisms and mitigation strategies, Journal of Power Sources, 184 (2008) 104-119.

[10] D.R. Lide, CRC handbook of chemistry and physics, CRC press2004.

[11] J.-M. Le Canut, R.M. Abouatallah, D.A. Harrington, Detection of membrane drying, fuel cell flooding, and anode catalyst poisoning on PEMFC stacks by electrochemical impedance spectroscopy, Journal of The Electrochemical Society, 153 (2006) A857.

[12] W. He, G. Lin, T. Van Nguyen, Diagnostic tool to detect electrode flooding in proton-exchange-membrane fuel cells, AIChE Journal, 49 (2003) 3221-3228.

[13] T.E. Springer, T. Zawodzinski, S. Gottesfeld, Polymer electrolyte fuel cell model, Journal of the electrochemical society, 138 (1991) 2334.

[14] F.N. Büchi, S. Srinivasan, Operating proton exchange membrane fuel cells without external humidification of the reactant gases: Fundamental aspects, Journal of the Electrochemical Society, 144 (1997) 2767.

[15] G. Hinds, Performance and durability of PEM fuel cells: a review, DOI (2004).

[16] A. Faghri, Z. Guo, Challenges and opportunities of thermal management issues related to fuel cell technology and modeling, International Journal of Heat and Mass Transfer, 48 (2005) 3891-3920.

[17] Q. Yan, H. Toghiani, Y.-W. Lee, K. Liang, H. Causey, Effect of sub-freezing temperatures on a PEM fuel cell performance, startup and fuel cell components, Journal of Power Sources, 160 (2006) 1242-1250.

[18] S. He, S.H. Kim, M.M. Mench, 1D transient model for frost heave in polymer electrolyte fuel cells: II. Parametric study, Journal of The Electrochemical Society, 154 (2007) B1024.

[19] S. Kim, B.K. Ahn, M. Mench, Physical degradation of membrane electrode assemblies undergoing freeze/thaw cycling: Diffusion media effects, Journal of Power Sources, 179 (2008) 140-146.

[20] B. Kienitz, H. Baskaran, T. Zawodzinski, B. Pivovar, A half cell model to study performance degradation of a PEMFC due to cationic contamination, ECS Transactions, 11 (2007) 777.

[21] J. Baschuk, X. Li, Carbon monoxide poisoning of proton exchange membrane fuel cells, International Journal of Energy Research, 25 (2001) 695-713.

[22] R.L. Borup, J.R. Davey, F.H. Garzon, D.L. Wood, M.A. Inbody, PEM fuel cell electrocatalyst durability measurements, Journal of Power Sources, 163 (2006) 76-81.

[23] R. Makharia, S. Kocha, P. Yu, M.A. Sweikart, W. Gu, F. Wagner, H.A. Gasteiger, Durable PEM fuel cell electrode materials: Requirements and benchmarking methodologies, Ecs Transactions, 1 (2006) 3.

[24] R.M. Darling, J.P. Meyers, Kinetic model of platinum dissolution in PEMFCs, Journal of the Electrochemical Society, 150 (2003) A1523.

[25] W. Gu, R.N. Carter, T.Y. Paul, H.A. Gasteiger, Start/stop and local H2 starvation mechanisms of carbon corrosion: model vs. experiment, ECS transactions, 11 (2007) 963.

[26] T.Y. Paul, W. Gu, R. Makharia, F.T. Wagner, H.A. Gasteiger, The impact of carbon stability on PEM fuel cell startup and shutdown voltage degradation, Ecs Transactions, 3 (2006) 797.

[27] W. Bi, G.E. Gray, T.F. Fuller, PEM fuel cell Pt∕C dissolution and deposition in nafion electrolyte, Electrochemical and Solid-State Letters, 10 (2007) B101.

[28] R.M. Darling, J.P. Meyers, Mathematical model of platinum movement in PEM fuel cells, Journal of the Electrochemical Society, 152 (2004) A242.

[29] A. Shah, T. Ralph, F. Walsh, Modeling and simulation of the degradation of perfluorinated ion-exchange membranes in PEM fuel cells, Journal of The Electrochemical Society, 156 (2009) B465.

[30] A.A. Franco, R. Coulon, R.F. de Morais, S.K. Cheah, A. Kachmar, M.A. Gabriel, Multi-scale modeling-based prediction of PEM Fuel Cells MEA durability under automotive operating conditions, ECS Transactions, 25 (2009) 65.

[31] A. Ohma, S. Yamamoto, K. Shinohara, Membrane degradation mechanism during open-circuit voltage hold test, Journal of Power Sources, 182 (2008) 39-47.

[32] S. Kundu, M.W. Fowler, L.C. Simon, R. Abouatallah, N. Beydokhti, Degradation analysis and modeling of reinforced catalyst coated membranes operated under OCV conditions, Journal of Power Sources, 183 (2008) 619-628.

[33] A. Bose, P. Babburi, R. Kumar, D. Myers, J. Mawdsley, J. Milhuff, Performance of individual cells in polymer electrolyte membrane fuel cell stack under-load cycling conditions, Journal of Power Sources, 243 (2013) 964-972.

[34] K. Cooper, M. Smith, Electrical test methods for on-line fuel cell ohmic resistance measurement, Journal of Power Sources, 160 (2006) 1088-1095.

[35] T. Madden, D. Weiss, N. Cipollini, D. Condit, M. Gummalla, S. Burlatsky, V. Atrazhev, Degradation of polymer-electrolyte membranes in fuel cells: I. experimental, Journal of The Electrochemical Society, 156 (2009) B657.

[36] D. Liu, S. Case, Durability study of proton exchange membrane fuel cells under dynamic testing conditions with cyclic current profile, Journal of Power Sources, 162 (2006) 521-531.

[37] M. Inaba, T. Kinumoto, M. Kiriake, R. Umebayashi, A. Tasaka, Z. Ogumi, Gas crossover and membrane degradation in polymer electrolyte fuel cells, Electrochimica Acta, 51 (2006) 5746-5753.

[38] A. Pandy, Z. Yang, M. Gummalla, V.V. Atrazhev, N.Y. Kuzminyh, V.I. Sultanov, S. Burlatsky, A carbon corrosion model to evaluate the effect of steady state and transient operation of a polymer electrolyte membrane fuel cell, Journal of the Electrochemical Society, 160 (2013) F972.

[39] H. Tang, Z. Qi, M. Ramani, J.F. Elter, PEM fuel cell cathode carbon corrosion due to the formation of air/fuel boundary at the anode, Journal of Power Sources, 158 (2006) 1306-1312.

[40] C.A. Reiser, L. Bregoli, T.W. Patterson, S.Y. Jung, J.D. Yang, M.L. Perry, T.D. Jarvi, A reverse-current decay mechanism for fuel cells, Electrochemical and Solid-State Letters, 8 (2005) A273.

[41] N. Takeuchi, T. Fuller, Modeling of transient state carbon corrosion for PEMFC electrodes, ECS Transactions, 11 (2007) 1021.

[42] J.P. Meyers, R.M. Darling, Model of carbon corrosion in PEM fuel cells, Journal of the Electrochemical Society, 153 (2006) A1432.

[43] W. Schmittinger, A. Vahidi, A review of the main parameters influencing long-term performance and durability of PEM fuel cells, Journal of power sources, 180 (2008) 1-14.

[44] P.W. Voorhees, The theory of Ostwald ripening, Journal of Statistical Physics, 38 (1985) 231-252.

[45] N.M. Vichare, M.G. Pecht, Prognostics and health management of electronics, IEEE transactions on components and packaging technologies, 29 (2006) 222-229.

[46] D.A. Tobon-Mejia, K. Medjaher, N. Zerhouni, G. Tripot, A data-driven failure prognostics method based on mixture of Gaussians hidden Markov models, IEEE Transactions on reliability, 61 (2012) 491-503.

[47] M.A. Van Gerven, B.G. Taal, P.J. Lucas, Dynamic Bayesian networks as prognostic models for clinical patient management, Journal of biomedical informatics, 41 (2008) 515-529.

[48] J.M. Karandikar, N.H. Kim, T.L. Schmitz, Prediction of remaining useful life for fatigue-damaged structures using Bayesian inference, Engineering Fracture Mechanics, 96 (2012) 588-605.

[49] T. Benkedjouh, K. Medjaher, N. Zerhouni, S. Rechak, Health assessment and life prediction of cutting tools based on support vector regression, Journal of intelligent manufacturing, 26 (2015) 213-223.

[50] W.Q. Wang, M.F. Golnaraghi, F. Ismail, Prognosis of machine health condition using neuro-fuzzy systems, Mechanical Systems and Signal Processing, 18 (2004) 813-831.

[51] G. Vachtsevanos, P. Wang, Fault prognosis using dynamic wavelet neural networks, 2001 ieee autotestcon proceedings. ieee systems readiness technology conference.(cat. no. 01ch37237), IEEE, 2001, pp. 857-870.

[52] S. Saon, T. Hiyama, Predicting remaining useful life of rotating machinery based artificial neural network, Computers & Mathematics with Applications, 60 (2010) 1078-1087.

[53] R. Huang, L. Xi, X. Li, C.R. Liu, H. Qiu, J. Lee, Residual life predictions for ball bearings based on self-organizing map and back propagation neural network methods, Mechanical systems and signal processing, 21 (2007) 193-207.

[54] R. Gouriveau, N. Zerhouni, Connexionist-systems-based long term prediction approaches for prognostics, IEEE Transactions on Reliability, 61 (2012) 909-920.

[55] J.Z. Sikorska, M. Hodkiewicz, L. Ma, Prognostic modelling options for remaining useful life estimation by industry, Mechanical systems and signal processing, 25 (2011) 1803-1836.

[56] G. Niu, B.-S. Yang, Dempster–Shafer regression for multi-step-ahead time-series prediction towards data-driven machinery prognosis, Mechanical systems and signal processing, 23 (2009) 740-751.

[57] S. Uckun, K. Goebel, P.J. Lucas, Standardizing research methods for prognostics, 2008 International Conference on Prognostics and Health Management, IEEE, 2008, pp. 1-10.

[58] J. Qiu, B.B. Seth, S.Y. Liang, C. Zhang, Damage mechanics approach for bearing lifetime prognostics, Mechanical systems and signal processing, 16 (2002) 817-829.

[59] M. Pecht, J. Gu, Physics-of-failure-based prognostics for electronic products, Transactions of the Institute of Measurement and Control, 31 (2009) 309-322.

[60] J. Luo, K.R. Pattipati, L. Qiao, S. Chigusa, Model-based prognostic techniques applied to a suspension system, IEEE Transactions on Systems, Man, and Cybernetics-Part A: Systems and Humans, 38 (2008) 1156-1168.

[61] C.J. Li, H. Lee, Gear fatigue crack prognosis using embedded model, gear dynamic model and fracture mechanics, Mechanical systems and signal processing, 19 (2005) 836-846.

[62] G. Kacprzynski, A. Sarlashkar, M. Roemer, A. Hess, B. Hardman, Predicting remaining life by fusing the physics of failure modeling with diagnostics, JOm, 56 (2004) 29-35.

[63] M.G. Pecht, A prognostics and health management roadmap for information and electronics-rich systems, IEICE ESS Fundamentals Review, 3 (2010) 4_25-24_32.

[64] S. Kumar, M. Torres, Y. Chan, M. Pecht, A hybrid prognostics methodology for electronic products, 2008 IEEE international joint conference on neural networks (IEEE world congress on computational intelligence), IEEE, 2008, pp. 3479-3485.

[65] M.L. Thompson, M.A. Kramer, Modeling chemical processes using prior knowledge and neural networks, AIChE Journal, 40 (1994) 1328-1340.

[66] M. Chen, U. Challita, W. Saad, C. Yin, M. Debbah, Artificial neural networks-based machine learning for wireless networks: A tutorial, IEEE Communications Surveys & Tutorials, 21 (2019) 3039-3071.

[67] A.S. Tenney, M.N. Glauser, C.J. Ruscher, Z.P. Berger, Application of artificial neural networks to stochastic estimation and jet noise modeling, AIAA journal, DOI (2020).

[68] M. Tkáč, R. Verner, Artificial neural networks in business: Two decades of research, Applied Soft Computing, 38 (2016) 788-804.

[69] F. Ahmadzadeh, J. Lundberg, Remaining useful life estimation, International Journal of System Assurance Engineering and Management, 5 (2014) 461-474.

[70] J. Wang, Y. Ma, L. Zhang, R.X. Gao, D. Wu, Deep learning for smart manufacturing: Methods and applications, Journal of manufacturing systems, 48 (2018) 144-156.

[71] P. Ongsulee, Artificial intelligence, machine learning and deep learning, 2017 15th international conference on ICT and knowledge engineering (ICT&KE), IEEE, 2017, pp. 1-6.

[72] A.I. Károly, R. Fullér, P. Galambos, Unsupervised clustering for deep learning: A tutorial survey, Acta Polytechnica Hungarica, 15 (2018) 29-53.

[73] Y. Jaafra, J.L. Laurent, A. Deruyver, M.S. Naceur, A review of meta-reinforcement learning for deep neural networks architecture search, arXiv preprint arXiv:1812.07995, DOI (2018).

[74] S. Khan, T. Yairi, A review on the application of deep learning in system health management, Mechanical Systems and Signal Processing, 107 (2018) 241-265.

[75] R. Zhao, R. Yan, Z. Chen, K. Mao, P. Wang, R.X. Gao, Deep learning and its applications to machine health monitoring, Mechanical Systems and Signal Processing, 115 (2019) 213-237.

[76] S. Trenn, Multilayer perceptrons: Approximation order and necessary number of hidden units, IEEE transactions on neural networks, 19 (2008) 836-844.

[77] X. Li, Q. Ding, J.-Q. Sun, Remaining useful life estimation in prognostics using deep convolution neural networks, Reliability Engineering & System Safety, 172 (2018) 1-11.

[78] H. Faris, I. Aljarah, S. Mirjalili, Training feedforward neural networks using multi-verse optimizer for binary classification problems, Applied Intelligence, 45 (2016) 322-332.

[79] J. Feng, S. Lu, Performance analysis of various activation functions in artificial neural networks, Journal of physics: conference series, IOP Publishing, 2019, pp. 022030.

[80] H. Ramchoun, Y. Ghanou, M. Ettaouil, M.A. Janati Idrissi, Multilayer perceptron: Architecture optimization and training, DOI (2016).

[81] S. Basu, N. Das, R. Sarkar, M. Kundu, M. Nasipuri, D.K. Basu, An MLP based Approach for Recognition of HandwrittenBangla'Numerals, arXiv preprint arXiv:1203.0876, DOI (2012).

[82] P. Naraei, A. Abhari, A. Sadeghian, Application of multilayer perceptron neural networks and support vector machines in classification of healthcare data, 2016 Future Technologies Conference (FTC), IEEE, 2016, pp. 848-852.

[83] D. Das, A.K. Tripathi, A. Shah, S. Mehta, Application of Multilayer Perceptron for Forecasting of Selected IIPs of India–An Empirical Analysis, International Journal of Computer Sciences and Engineering, 6 (2018).

[84] O.B. Sezer, A.M. Ozbayoglu, E. Dogdu, An artificial neural network-based stock trading system using technical analysis and big data framework, proceedings of the southeast conference, 2017, pp. 223-226.

[85] J. Kim, J. Yu, M. Kim, K. Kim, S. Han, Estimation of Li-ion battery state of health based on multilayer perceptron: As an EV application, IFAC-PapersOnLine, 51 (2018) 392-397.

[86] Ł. Jedliński, J. Jonak, Early fault detection in gearboxes based on support vector machines and multilayer perceptron with a continuous wavelet transform, Applied Soft Computing, 30 (2015) 636-641.

[87] X. Hu, J. Vian, J.R. Slepski, D.C. Wunsch, Vibration analysis via neural network inverse models to determine aircraft engine unbalance condition, Proceedings of the International Joint Conference on Neural Networks, 2003., IEEE, 2003, pp. 3001-3006.

[88] L.F. de Almeida, J.W. Bizarria, F.C. Bizarria, M.H. Mathias, Condition-based monitoring system for rolling element bearing using a generic multi-layer perceptron, Journal of Vibration and Control, 21 (2015) 3456-3464.

[89] O. Geramifard, J.-X. Xu, C.K. Pang, J. Zhou, X. Li, Data-driven approaches in health condition monitoring—a comparative study, IEEE ICCA 2010, IEEE, 2010, pp. 1618-1622.

[90] I. Loboda, Y. Feldshteyn, V. Ponomaryov, Neural networks for gas turbine fault identification: multilayer perceptron or radial basis network?, Turbo Expo: Power for Land, Sea, and Air, 2011, pp. 465-475.

[91] S. Zolfaghari, S.B.M. Noor, M. Rezazadeh Mehrjou, M.H. Marhaban, N. Mariun, Broken rotor bar fault detection and classification using wavelet packet signature analysis based on fourier transform and multi-layer perceptron neural network, Applied Sciences, 8 (2017) 25.

[92] M. Heidari, S. Shateyi, Wavelet support vector machine and multi-layer perceptron neural network with continues wavelet transform for fault diagnosis of gearboxes, Journal of VIBROENGINEERING, 19 (2017) 125-137.

[93] A. Sherstinsky, Fundamentals of Recurrent Neural Network (RNN) and Long Short-Term Memory (LSTM) Network. eprint, arXiv preprint arXiv:1808.03314, DOI (2018).

[94] S. Rashka, V. Mirdzhalili, Machine Learning and Deep Learning with Python, scikit-learn, and TensorFlow 2, Birmingham, Mumbai. Packt, DOI (2020).

[95] M. Schuster, K.K. Paliwal, Bidirectional recurrent neural networks, IEEE transactions on Signal Processing, 45 (1997) 2673-2681.

[96] F.A. Gers, J. Schmidhuber, F. Cummins, Learning to forget: Continual prediction with LSTM, Neural computation, 12 (2000) 2451-2471.

[97] A. Graves, J. Schmidhuber, Framewise phoneme classification with bidirectional LSTM and other neural network architectures, Neural networks, 18 (2005) 602-610.

[98] A. Bhardwaj, W. Di, J. Wei, Deep Learning Essentials: Your hands-on guide to the fundamentals of deep learning and neural network modeling, Packt Publishing Ltd2018.

[99] R.C. Staudemeyer, E.R. Morris, Understanding LSTM--a tutorial into long short-term memory recurrent neural networks, arXiv preprint arXiv:1909.09586, DOI (2019).

[100] T. Fischer, C. Krauss, Deep learning with long short-term memory networks for financial market predictions, European journal of operational research, 270 (2018) 654-669.

[101] J. Lei, C. Liu, D. Jiang, Fault diagnosis of wind turbine based on Long Short-term memory networks, Renewable energy, 133 (2019) 422-432.

[102] Q. You, H. Jin, Z. Wang, C. Fang, J. Luo, Image captioning with semantic attention, Proceedings of the IEEE conference on computer vision and pattern recognition, 2016, pp. 4651-4659.

[103] L. Sun, T. Su, C. Liu, R. Wang, Deep LSTM networks for online Chinese handwriting recognition, 2016 15th international conference on frontiers in handwriting recognition (icfhr), IEEE, 2016, pp. 271-276.

[104] M. Baccouche, F. Mamalet, C. Wolf, C. Garcia, A. Baskurt, Sequential deep learning for human action recognition, Human Behavior Understanding: Second International Workshop, HBU 2011, Amsterdam, The Netherlands, November 16, 2011. Proceedings 2, Springer, 2011, pp. 29-39.

[105] J. Chen, D. Wang, Long short-term memory for speaker generalization in supervised speech separation, The Journal of the Acoustical Society of America, 141 (2017) 4705-4714.

[106] M. Sundermeyer, H. Ney, R. Schlüter, From feedforward to recurrent LSTM neural networks for language modeling, IEEE/ACM Transactions on Audio, Speech, and Language Processing, 23 (2015) 517-529.

[107] S. Zheng, K. Ristovski, A. Farahat, C. Gupta, Long short-term memory network for remaining useful life estimation, 2017 IEEE international conference on prognostics and health management (ICPHM), IEEE, 2017, pp. 88-95.

[108] Y. Wu, M. Yuan, S. Dong, L. Lin, Y. Liu, Remaining useful life estimation of engineered systems using vanilla LSTM neural networks, Neurocomputing, 275 (2018) 167-179.

[109] P. Malhotra, V. Tv, A. Ramakrishnan, G. Anand, L. Vig, P. Agarwal, G. Shroff, Multi-sensor prognostics using an unsupervised health index based on LSTM encoder-decoder, arXiv preprint arXiv:1608.06154, DOI (2016).

[110] Y. Zhou, Y. Huang, J. Pang, K. Wang, Remaining useful life prediction for supercapacitor based on long short-term memory neural network, Journal of Power Sources, 440 (2019) 227149.

[111] J. Liu, Q. Li, W. Chen, Y. Yan, Y. Qiu, T. Cao, Remaining useful life prediction of PEMFC based on long short-term memory recurrent neural networks, International Journal of Hydrogen Energy, 44 (2019) 5470-5480.

[112] F. Wang, X. Liu, G. Deng, X. Yu, H. Li, Q. Han, Remaining life prediction method for rolling bearing based on the long short-term memory network, Neural processing letters, 50 (2019) 2437-2454.

[113] J. Wu, K. Hu, Y. Cheng, H. Zhu, X. Shao, Y. Wang, Data-driven remaining useful life prediction via multiple sensor signals and deep long short-term memory neural network, ISA transactions, 97 (2020) 241-250.

[114] M. Jouin, R. Gouriveau, D. Hissel, M.-C. Péra, N. Zerhouni, Prognostics of PEM fuel cell in a particle filtering framework, International Journal of Hydrogen Energy, 39 (2014) 481-494.

[115] S. Morando, S. Jemei, R. Gouriveau, N. Zerhouni, D. Hissel, Fuel cells remaining useful lifetime forecasting using echo state network, 2014 IEEE vehicle power and propulsion conference (VPPC), IEEE, 2014, pp. 1-6.

[116] R. Silva, R. Gouriveau, S. Jemei, D. Hissel, L. Boulon, K. Agbossou, N.Y. Steiner, Proton exchange membrane fuel cell degradation prediction based on adaptive neuro-fuzzy inference systems, International Journal of Hydrogen Energy, 39 (2014) 11128-11144.

[117] W.O.L. Vianna, I.P. de Medeiros, B.S. Aflalo, L.R. Rodrigues, J.P.P. Malère, Proton exchange membrane fuel cells (PEMFC) impedance estimation using regression analysis, 2014 International Conference on Prognostics and Health Management, IEEE, 2014, pp. 1-8.

[118] A. Hochstein, H.-I. Ahn, Y.T. Leung, M. Denesuk, Switching vector autoregressive models with higher-order regime dynamics application to prognostics and health management, 2014 International conference on prognostics and health Management, IEEE, 2014, pp. 1-10.

[119] J.K. Kimotho, T. Meyer, W. Sextro, PEM fuel cell prognostics using particle filter with model parameter adaptation, 2014 International conference on prognostics and health management, IEEE, 2014, pp. 1-6.

[120] T. Kim, H. Kim, J. Ha, K. Kim, J. Youn, J. Jung, B.D. Youn, A degenerated equivalent circuit model and hybrid prediction for state-of-health (SOH) of PEM fuel cell, 2014 International Conference on Prognostics and Health Management, IEEE, 2014, pp. 1-7.

[121] E. Lechartier, E. Laffly, M.-C. Péra, R. Gouriveau, D. Hissel, N. Zerhouni, Proton exchange membrane fuel cell behavioral model suitable for prognostics, International Journal of Hydrogen Energy, 40 (2015) 8384-8397.

[122] M. Bressel, M. Hilairet, D. Hissel, B.O. Bouamama, Extended Kalman filter for prognostic of proton exchange membrane fuel cell, Applied Energy, 164 (2016) 220-227.

[123] M. Bressel, M. Hilairet, D. Hissel, B.O. Bouamama, Remaining useful life prediction and uncertainty quantification of proton exchange membrane fuel cell under variable load, IEEE Transactions on Industrial Electronics, 63 (2016) 2569-2577.

[124] K. Javed, R. Gouriveau, N. Zerhouni, D. Hissel, Data-driven Prognostics of Proton Exchange Membrane Fuel Cell Stack with constraint based Summation-Wavelet Extreme Learning Machine, International Conference on Fundamentals and Development of Fuel Cells, 2015.